

## 7. Part C of Task 1: case definition

### 7.1 Introduction

The purpose of this chapter is to define the modelling exercise for Part C. Rock and bentonite properties were defined in detail in the previous case definitions for Parts A and B (cf. Chapters 3 and 5) and will not be repeated here. Some details on the installation of rock sensors around the FEBEX drift will be given in section 7.2 and section 7.3 defines the results required for the modelling exercise.

### 7.2 Rock instrumentation around the FEBEX drift

Sensors whose response will be predicted for Part C were all installed in 19 radial (or close to radial) small diameter boreholes from the FEBEX drift. The three-dimensional view of all the boreholes drilled is shown in Figure 3.2, together with the Cartesian coordinate system. The origin is located at the intersection of the tunnel axis and the contact plane between the concrete plug and the bentonite buffer. Positive X axis is directed along the tunnel axis towards the other end of the test section. The Z axis is vertical, pointing upwards and the Y axis is perpendicular to the (XZ) plane. The position of all boreholes, their lengths and their diameters were given in the case definition for Part A (cf. Tables 3.1 and 3.2).

The co-ordinate system used in the Grimsel Test Site is the Swiss co-ordinate system. In order to define a point, use is made of east, north and height above the sea level. In order to define the direction of a line, use is made of the azimuth (angle formed by the projection of the line onto the horizontal plane with the north) and the inclination (angle formed by the line with the vertical plane) (cf. Figure 3.1).

The coding of the boreholes is consistent with the definition and naming of instrumented cross sections within the bentonite buffer. These sections are defined in Figures 5.2-5.7 of the case definition for Part B. The general coding of boreholes agrees with the following convention: S An m, where S stands for Section, An refers to the particular cross section (E1, E2, D1, D2, etc., with some sections have a single letter designation (L, N, G, H, I)), and m identifies the number of the borehole drilled in Section An. A maximum of 4 boreholes were drilled in a single section.

A total of 261 sensors were installed within the rock. They are indicated in Table 7.1 under the column G (Granite). Most of the sensors listed in Table 3 were located within the set of 19 boreholes mentioned. In addition, boreholes BOUS-1, BOUS-2, FBX-1 and FBX-2 drilled from the access tunnel were also used to locate some measuring instruments as described in the case definition for Part A. Finally, small diameter holes were also drilled from the FEBEX tunnel in order to locate within the granite, in the vicinity of the rock-bentonite interphase, a number of TDR probes and psychrometers. The following measured variables will be selected for the prediction exercise.

Table 7.1: Installed sensors (G: granite; B: bentonite; C: heater; S: service zone).

Variable (or instrument)	type of sensor	area				total
		G	B	C	S	
Temperature	Thermocouple	62	91	36		189
Total pressure in borehole in rock (3-D)	Vibrating wire	4				4
Total pressure on rock surface	Vibrating wire	30				30
Total pressure on heater	Vibrating wire		6			6
Hydraulic pressure in borehole in rock	Piezoresistive	62				62
Packer pressure in borehole	Piezoresistive	62				62
Pore pressure in bentonite	Vibrating wire		52			52
Water content	Capacitive		58		1	59
Water content	Psychrometer	28	48			76
Water content	TDR	4	20			24
Extensometer in rock	Vibrating wire	2x3				6
Heater displacement	Vibrating wire		9			9
Expansion of bentonite block	Vibrating wire		8			8
Displacement within the bentonite barrier	Potentiometer		2x3			6
Clinometer	LVDT		6x2			12
Crack meter	LVDT	1x3				3
Gas pressure in the bentonite barrier	Magnetic		4			4
Gas flow	Manual measure		6			6
Atmospheric pressure	Piezoresistive				1	1
Velocity of ventilation air	Hot wire				1	1
Resistor intensity	Electric converter				6	6
Resistor voltage	Electric converter				6	6
<b>TOTALS</b>		<b>261</b>	<b>320</b>	<b>36</b>	<b>15</b>	<b>632</b>

## 7.2.1 Temperature

T-type thermocouples were installed at different positions in the boreholes (other temperature sensors were integrated into other instruments for the sensors of temperature compensation). Thermocouples offer a good stability and accuracy. They are also protected against corrosion. Their temperature range is 0-350 °C.

## 7.2.2 Water pressure in rock boreholes

Sets of packers have been placed in all boreholes. This set-up divides the boreholes into measurement intervals (Figure 7.1). Hydraulic pressures at the intervals, limited by the packers, were measured by manometers by means of flexible tubes. Regular pressure transducers are then used to measure pressure.

## 7.2.3 Total normal stresses

Three normal components of stress are measured by means of total pressure cells. Four sets of 3 cells were prepared and grouted “in situ” in boreholes SG1 and SG2.

Each cell had five sensors oriented in different directions (see Figure 7.2) and fixed on a common support 2 m long. Each one of the sensors was a circular steel flat cell. An interpretation of the five readings provides the normal stress components in three directions: radial (with respect to the tunnel axis) ( $\sigma_r$ ), axial (along the direction of

tunnel axis) ( $\sigma_x$ ) and circumferential (normal to the radial direction ( $\sigma_\theta$ )). The installation of these cells required a special system of rods, packers and anchors (Figure 7.3). Once the sets were in position the borehole was filled with a slightly expansive mortar. Once the mortar was cured, cells were pressurized against the mass of surrounding mortar to guarantee a good initial contact in accordance with manufacturer specifications.

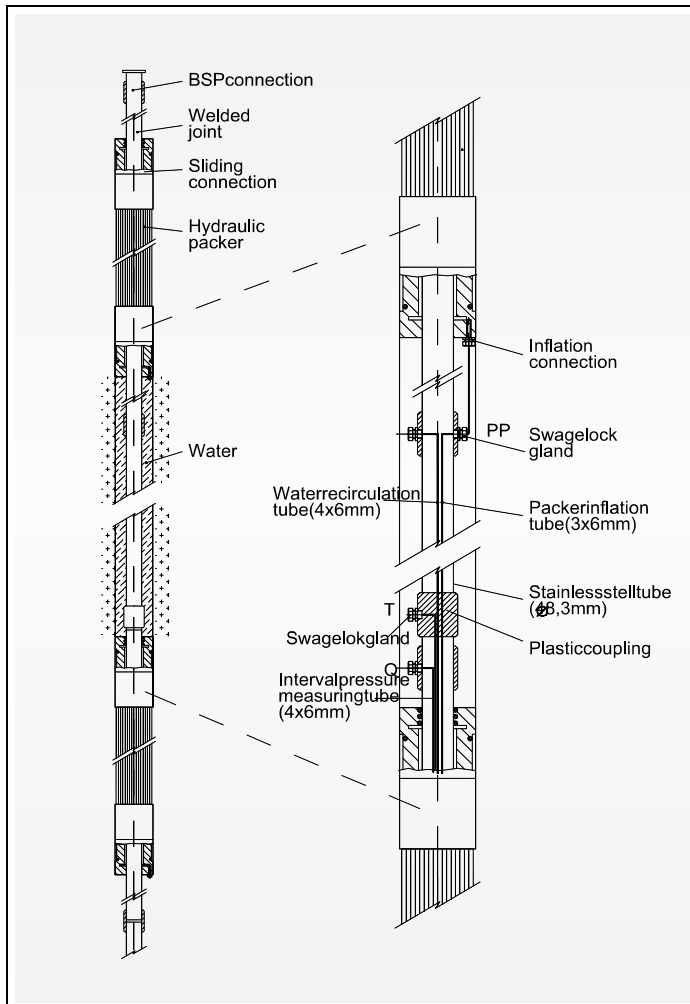


*Figure 7.1: Installation of hydrogeological measuring devices in granite boreholes.*



*Figure 7.2: Set of total pressure sensors for the three-dimensional measuring of stresses in boreholes in granite.*

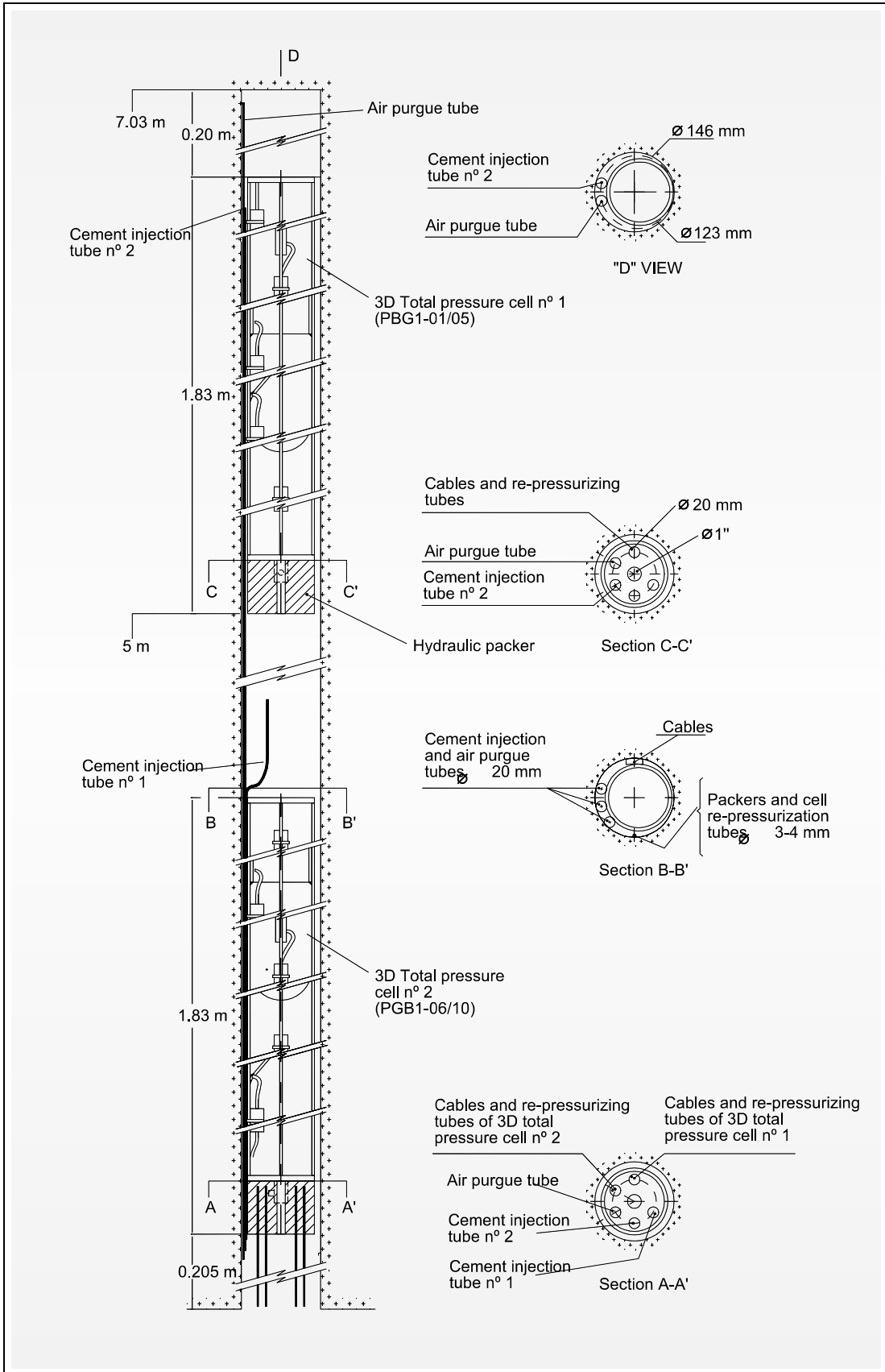
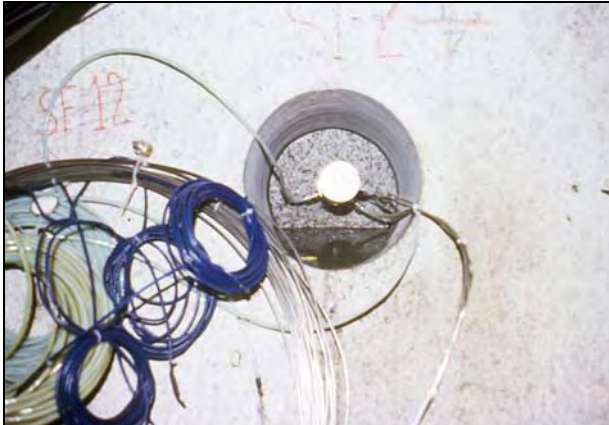


Figure 7.3: Method of emplacement of triaxial total pressure cells in borehole SG1.

## 7.2.4 Radial displacements

Radial displacements were measured by means of borehole extensometers installed in borings SI1 and SI2. They are located close to the position of the stress cells. Each parameter consists of the graphite rods with independent anchoring points located at a depth of 1.0, 3.0 and 7.0 m into the borehole. Transducers are grouped at the borehole entry and this set-up required an over-excavation to a diameter of 250 mm. Figures 7.4 and 7.5 show details of the installation.



*Figure 7.4: Head of one of the extensometers (borehole SI-2). Note the edges of water caused by the drilling process.*

## 7.2.5 Location of the sensors

The position of the sensors involved in this exercise is indicated in Figures 7.6-7.8. In these figures, the final co-ordinates (X, Y, Z) of sensors are also given. The co-ordinates refer to the central point of the measuring zone or interval. The co-ordinate system used was defined at the beginning of the present Section (see Figure 3.1).

Each sensor is identified by the following code: AA – BBn – CC, where represents the sensor type according to Table 7.1, BBn stands for the location according to the borehole coding already described, and CC is the order number of the sensor within the corresponding borehole.

## 7.3 Required results.

### 7.3.1 Work to be done.

Four types of results are required. They refer to:

- Evolution (in time) of temperature (T) in selected points at increasing radial distance.
- Evolution of water pressure ( $p_w$ ) in selected points at increasing radial distance.
- Evolution of normal stresses ( $\sigma_r$ ,  $\sigma_\theta$ ,  $\sigma_x$ ) in selected points at increasing radial distance.
- Evolution of radial displacements ( $u_r$ ) in selected points at increasing radial distance.
- Distribution of water pressure,  $p_w$ , along different radii for three selected times.

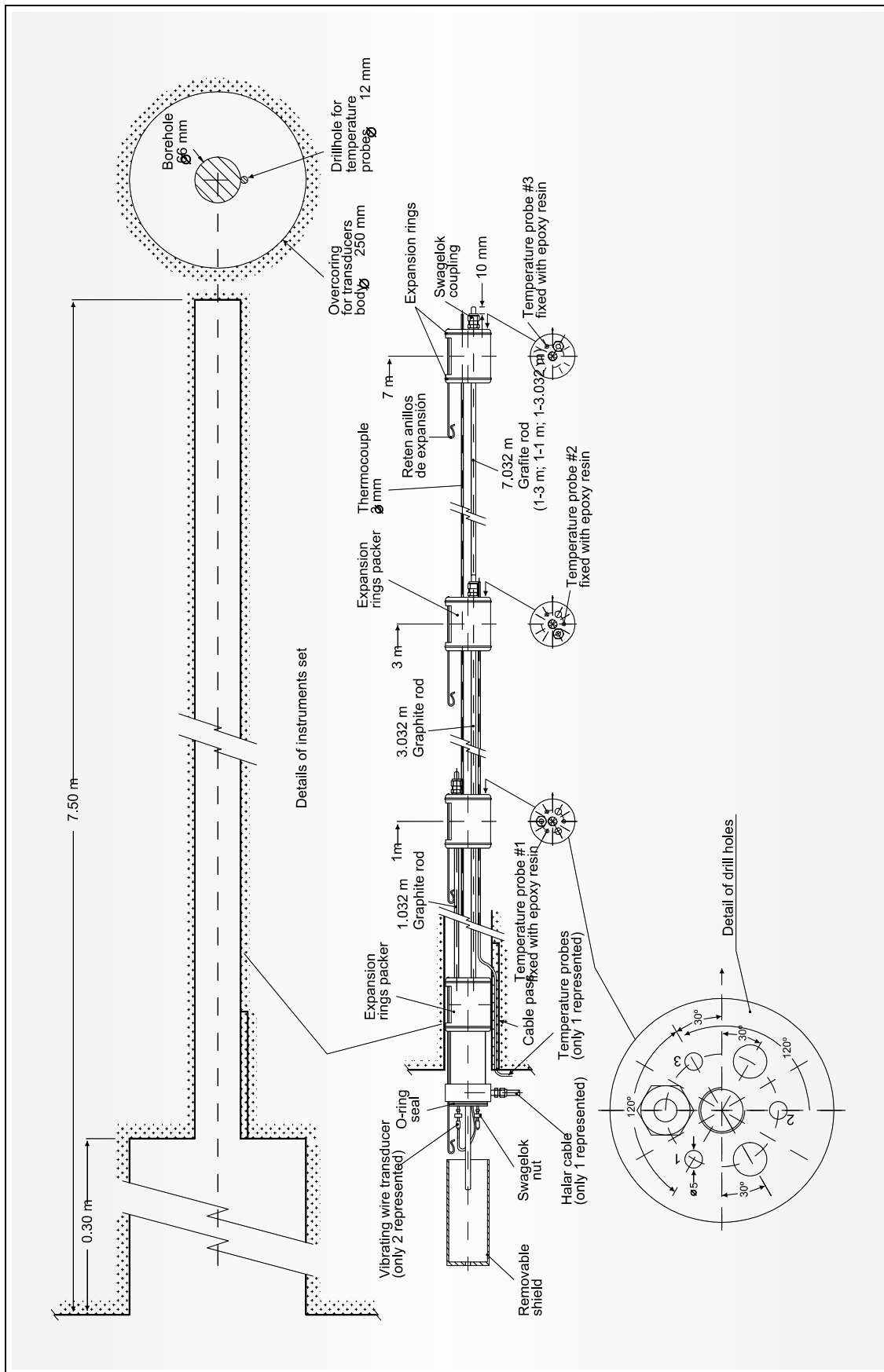


Figure 7.5: Method of emplacement of rod extensometers in the granite boreholes.

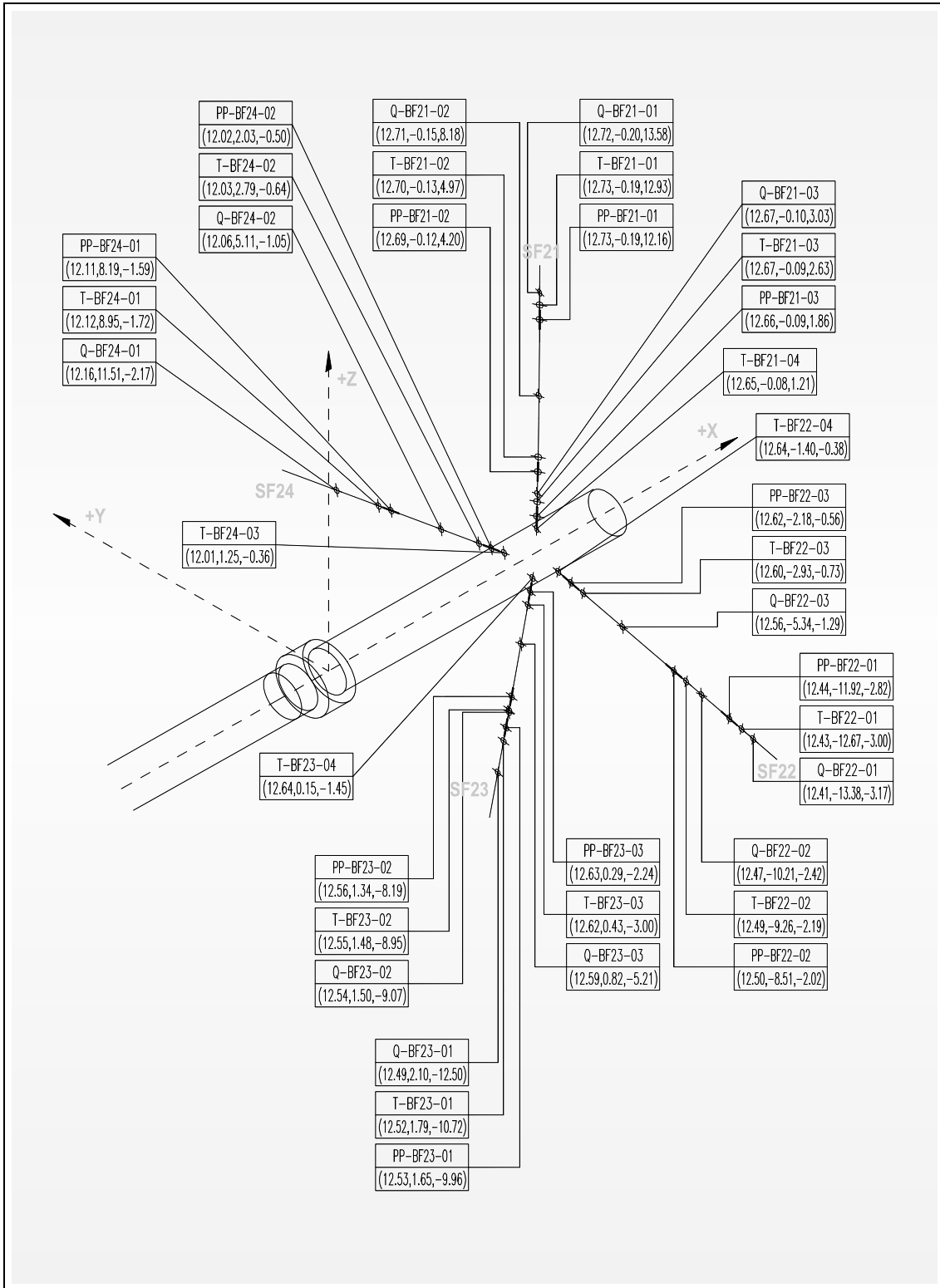


Figure 7.6: Final position of sensors in boreholes SF21, SF22, SF23 and SF24.

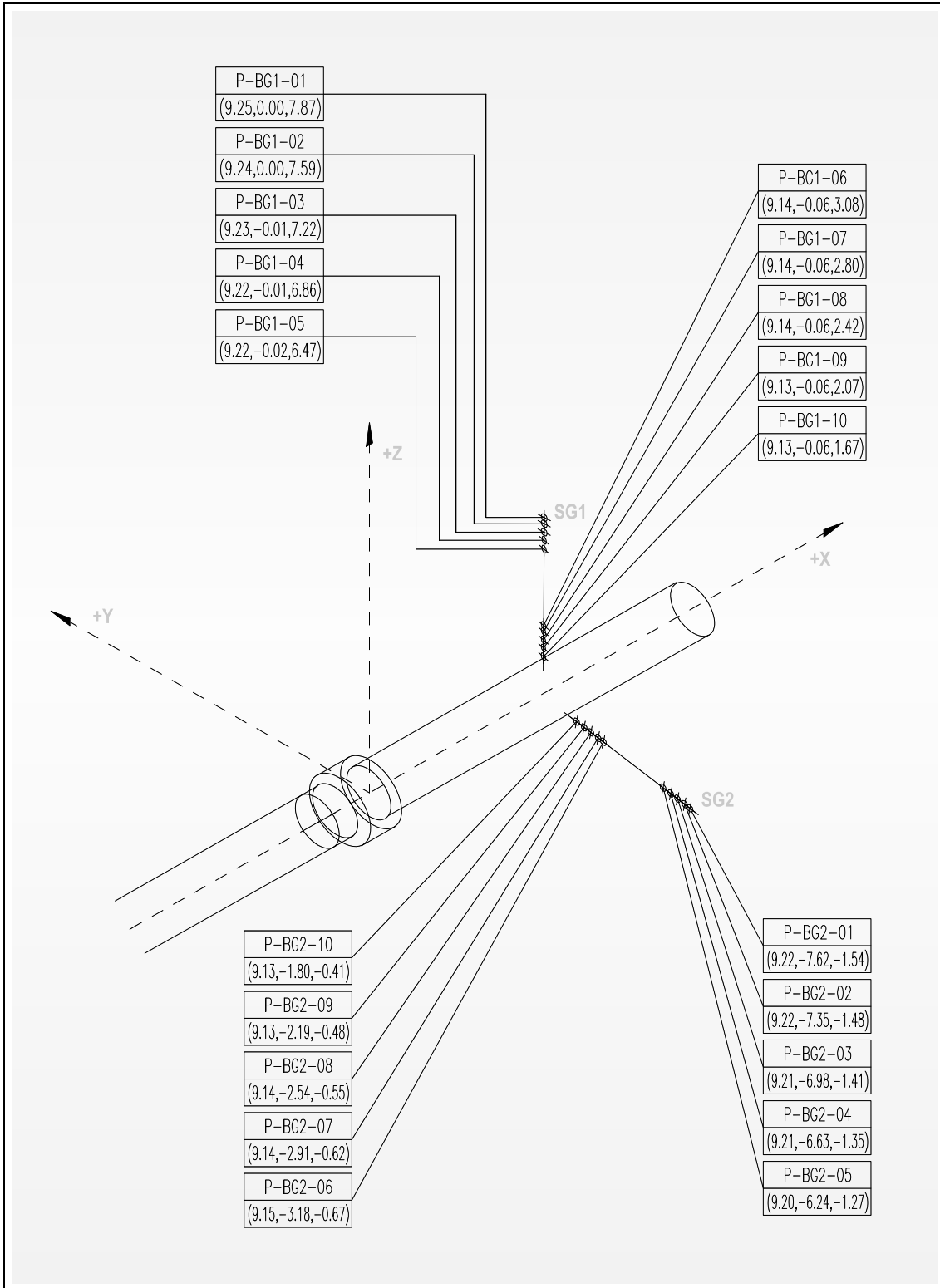


Figure 7.7: Final position of sensors in boreholes SG1 and SG2.

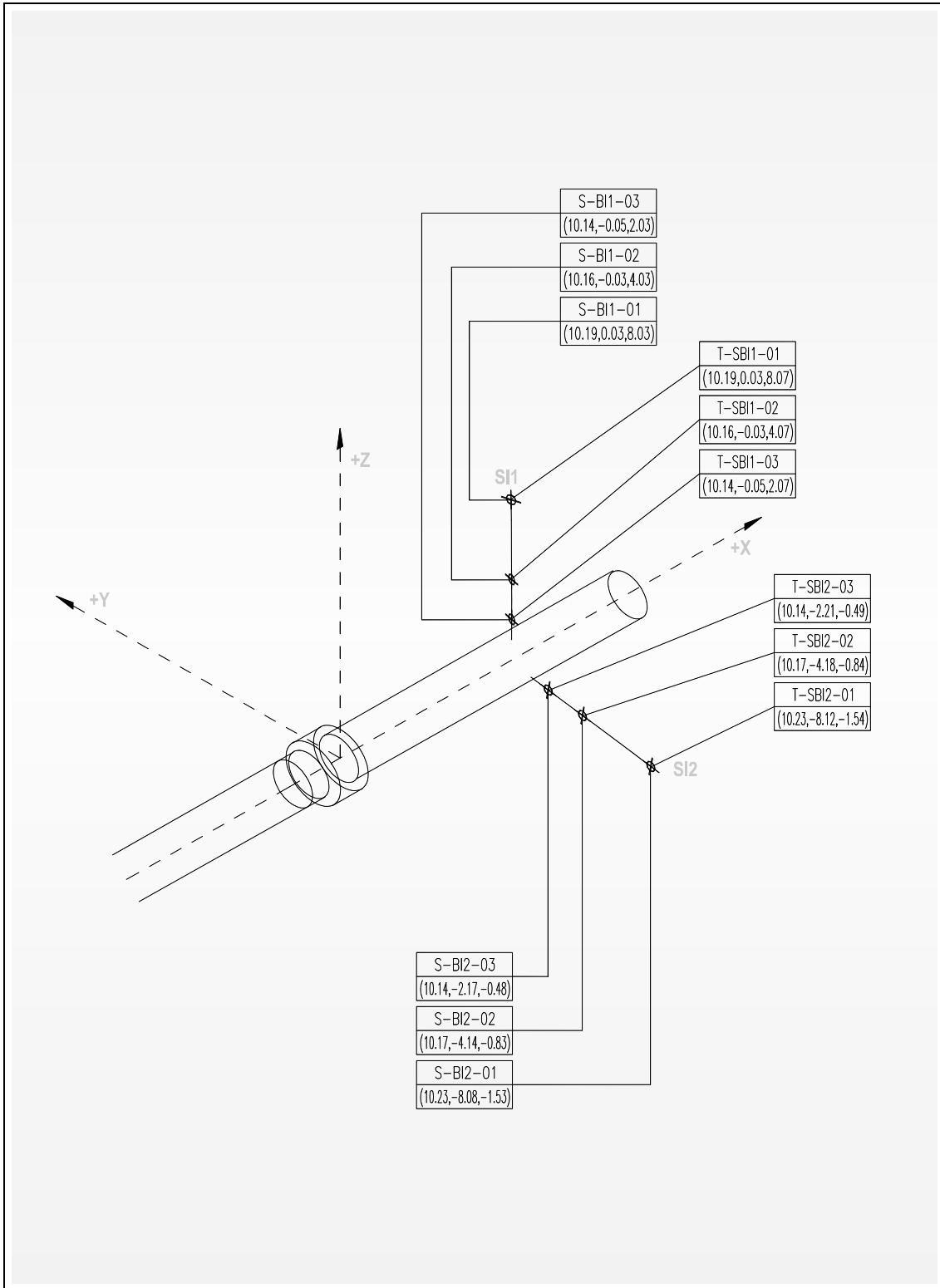


Figure 7.8: Final position of sensors in boreholes SI1 and SI2.



**Borehole SF21 (borehole entry located at X = 12.65 m)**

Point	Sensor coordinates (m)		
	X	Y	Z
1	12.67	-0.10	3.03
2	12.71	-0.15	8.18
3	12.72	-0.20	13.58

**Borehole SF22 (borehole entry located at X = 12.64 m)**

Point	Sensor coordinates (m)		
	X	Y	Z
1	12.56	-5.34	-1.29
2	12.47	-10.21	-2.42
3	12.41	-13.38	-3.17

**Borehole SF23 (borehole entry located at X = 12.64 m)**

Point	Sensor coordinates (m)		
	X	Y	Z
1	12.59	0.82	-5.21
2	12.54	1.50	-9.07
3	12.49	2.10	-12.50

**Borehole SF24 (borehole entry located at X = 12.01 m)**

Point	Sensor coordinates (m)		
	X	Y	Z
1	12.06	5.11	-1.05
2	12.16	11.51	-2.17

**7.3.4 Evolution of normal stresses ( $\sigma_r$ ,  $\sigma_\theta$ ,  $\sigma_x$ ) at selected points.**

The evolution of three normal components of stress within the period (Day 0 – Day 1000) is required at the following points:

**Borehole SG1 (borehole entry located at X = 9.13 m)**

Point	Stress	Sensor coordinates (m)		
		X	Y	Z
1	$\sigma_x$	9.14	-0.06	2.42
2	$\sigma_\theta$	9.14	-0.06	2.80
3	$\sigma_r$	9.14	-0.06	3.08
4	$\sigma_x$	9.23	-0.01	7.22
5	$\sigma_\theta$	9.24	0.00	7.59
6	$\sigma_r$	9.25	0.00	7.87

**Borehole SG2 (borehole entry located at X = 9.13 m)**

Point	Stress	Sensor coordinates (m)		
		X	Y	Z
1	$\sigma_x$	9.14	-2.54	-0.55
2	$\sigma_\theta$	9.14	-2.91	-0.62
3	$\sigma_r$	9.15	-3.18	-0.67
4	$\sigma_x$	9.20	-6.24	-1.27
5	$\sigma_\theta$	9.21	-6.63	-1.35
6	$\sigma_r$	9.21	-6.98	-1.41

**7.3.5 Evolution of radial displacements ( $u_r$ ) at selected points.**

The evolution of radial displacements within the period (Day 0 – Day 1000) is required at the following points:

**Borehole SI1 (borehole entry located at X = 10.14 m)**

Point	Anchor coordinates (m)		
	X	Y	Z
1	10.14	-0.05	2.03
2	10.16	-0.03	4.03
3	10.19	0.03	8.03

**Borehole SI2 (borehole entry located at X = 10.14 m)**

Point	Anchor coordinates (m)		
	X	Y	Z
1	10.14	-2.17	-0.48
2	10.17	-4.14	-0.83
3	10.23	-8.08	-1.53

**7.3.6 Distribution of water pressure,  $p_w$ , along different radii for three selected times.**

The distribution of water pressure along the boreholes SF21, SF22, SF23 and SF24 (see Figure 7.69) is required at the following times:

Time	days
T1	100
T2	600
T3	1000

**7.3.7 Output specifications.**

In order to locate points in the space, the cartesian system of coordinates used is represented in Figure 1 will be used. The origin is located on the intersection of the tunnel axis with the surface of the concrete plug in contact with the bentonite barrier.

The x-axis is directed along the tunnel axis and points towards the end of the tunnel, nearly to the west. The y-axis is horizontal and points nearly to the south. The z-axis is in the vertical plane that contains the x-axis and points upwards. In order to locate events on time, the origin of time will be on 27 February 1997 at 0:00.

The output data should conform with the document "General Specifications". The following points are recalled: (1) the modelling report should be put in the WinWord file "XXX1C.doc"; (2) output data should be put in the ASCII files "XXX1CNN.txt", where "XXX" stands for the participant's code and "NN" is the file number; (3) data should be arranged in a way similar to that shown in Figures 7.9 to 7.12; and (4) the points provided should be enough to properly define the evolution curve.

The 5 ASCII files where output data should be placed and their content are:

- XXX1C01.txt contains the temperature evolutions at the 8 (2 boreholes × 4 points) specified points.
- XXX1C02.txt contains the water pressure evolutions at the 11 (3 boreholes × 3 points + 1 borehole × 2 points) specified points.
- XXX1C03.txt contains the evolutions of a total stress component at the 12 (2 boreholes × 6 points) specified points.
- XXX1C04.txt radial displacement evolutions at 6 (2 boreholes × 3 points) specified points.
- XXX1C05.txt contains the water pressure distributions along 4 the specified boreholes and at the 3 selected times.

The units to employ in the output files are: (1) coordinates x, y, z in m; (2) time t in days; (3) temperature T in °C; (4) water pressure P in MPa; (5) total stress components s\_x in MPa; and (6) radial displacement u\_r in m. Concerning the sign conventions, the positive sign corresponds to (1) compressions for the total stress components; and (2) moving away from the FEBEX drift for radial displacements.

```

FILENAME      : XXX1C01.txt
PARTICIPANT   : Participant's identification
DATE          : DD.MM.YY

Temperature T (°C) evolutions

at point XX

x(m)  y(m)  z(m)  t(day)  T(°C)
0.000E+00  0.000E+00  0.000E+00  0.000E+00  0.000E+00
0.000E+00  0.000E+00  0.000E+00  0.000E+00  0.000E+00
...      ...      ...      ...      ...

at point XX

x(m)  y(m)  z(m)  t(day)  T(°C)
0.000E+00  0.000E+00  0.000E+00  0.000E+00  0.000E+00
0.000E+00  0.000E+00  0.000E+00  0.000E+00  0.000E+00
...      ...      ...      ...      ...

```

Figure 7.9: Example of output file "XXX1C1.txt".

```

FILENAME      : XXX1C02.txt
PARTICIPANT: Participant's identification
DATE         : DD.MM.YY

Water pressure P (MPa) evolutions

at point XX

x(m)  y(m)  z(m)  t(day)  P (MPa)
0.000E+00  0.000E+00  0.000E+00  0.000E+00  0.000E+00
0.000E+00  0.000E+00  0.000E+00  0.000E+00  0.000E+00
...      ...      ...      ...      ...

at point XX

x(m)  y(m)  z(m)  t(day)  P (MPa)
0.000E+00  0.000E+00  0.000E+00  0.000E+00  0.000E+00
0.000E+00  0.000E+00  0.000E+00  0.000E+00  0.000E+00
...      ...      ...      ...      ...

```

*Figure 7.10: Example of output file "XXX1C02.txt".*

```

FILENAME      : XXX1C03.txt
PARTICIPANT: Participant's identification
DATE         : DD.MM.YY

Total stress component s_x (axial, radial or tangential) (MPa)
evolutions

at point XX

x(m)  y(m)  z(m)  t(day)  s_x (MPa)
0.000E+00  0.000E+00  0.000E+00  0.000E+00  0.000E+00
0.000E+00  0.000E+00  0.000E+00  0.000E+00  0.000E+00
...      ...      ...      ...      ...

at point XX

x(m)  y(m)  z(m)  t(day)  s_x (MPa)
0.000E+00  0.000E+00  0.000E+00  0.000E+00  0.000E+00
0.000E+00  0.000E+00  0.000E+00  0.000E+00  0.000E+00
...      ...      ...      ...      ...

```

*Figure 7.11: Example of output file "XXX1C03.txt".*

```

FILENAME      : XXX1C04.txt
PARTICIPANT: Participant's identification
DATE         : DD.MM.YY

Radial displacement u_r (m) evolutions

at point XX

x(m)  y(m)  z(m)  t(day)  u_r(m)
0.000E+00  0.000E+00  0.000E+00  0.000E+00  0.000E+00
0.000E+00  0.000E+00  0.000E+00  0.000E+00  0.000E+00
...      ...      ...      ...      ...

at point XX

x(m)  y(m)  z(m)  t(day)  u_r(m)
0.000E+00  0.000E+00  0.000E+00  0.000E+00  0.000E+00
0.000E+00  0.000E+00  0.000E+00  0.000E+00  0.000E+00
...      ...      ...      ...      ...

```

*Figure 7.12: Example of output file "XXX1C04.txt".*

```

FILENAME      : XXX1C05.txt
PARTICIPANT: Participant's identification
DATE         : DD.MM.YY

Water pressure P (MPa) radial distributions

along borehole XX

x(m)  y(m)  z(m)  t= 100 d t= 600 d t= 1000d
0.000E+00  0.000E+00  0.000E+00  0.000E+00  0.000E+00  0.000E+00
0.000E+00  0.000E+00  0.000E+00  0.000E+00  0.000E+00  0.000E+00
...      ...      ...      ...      ...      ...

along borehole XX

x(m)  y(m)  z(m)  t= 100 d t= 600 d t= 1000d
0.000E+00  0.000E+00  0.000E+00  0.000E+00  0.000E+00  0.000E+00
0.000E+00  0.000E+00  0.000E+00  0.000E+00  0.000E+00  0.000E+00
...      ...      ...      ...      ...      ...

```

*Figure 7.13: Example of output file "XXX1C05.txt".*

## **8. Part C of Task 1: results and evaluation**

### **8.1 Introduction**

This report provides a description of the work performed for Part C of Task 1, DECOVALEX III Project. The general objective is the modelling of FEBEX “in situ” test, as a “blind” prediction exercise, focused on the thermo-hydro-mechanical analysis of the rock. Specifically, based on the characterization of the rock massif and on details of the process of test installation and performance, the rock response in the immediate vicinity of the buffer is required. The rock is subjected to the heat released by heaters and by swelling pressures resulting from bentonite hydration. The initial hydrological regime (as described and simulated in Part A) is also modified by the presence of the impervious barrier. Temperature, stresses, water pressures and displacements in selected points of the rock were required.

In subsequent sections, the modelling approaches followed by each team are briefly summarised, the physical phenomena relevant to the problem at hand are discussed and a comparison of the predictions submitted by the different teams is presented, whereby their computed results are compared with actual measurements. The reports produced by the teams provide a deeper insight in particular aspects of the computations performed. They are self-contained reports with a relatively common structure (mathematical setting, model calibration, numerical solution, additional comments, references) in order to facilitate cross comparisons.

### **8.2 Modelling teams**

From the ten teams involved in Task 1 of the DECOVALEX III Project, eight teams participated in Part C: ANG, BGR, CNS, DOE, IPS, JNC, SKB and SKI.

### **8.3 Modelling approaches**

In this Section we examine in a systematic way the main features of the work carried out by the various teams in order to understand their success in modelling the problem at hand. Our analysis is essentially based on the teams’ reports that are included as Annexes in the accompanying CD-ROM.

This section is structured as follows. First, we summarize the main features of the models used by the various teams. Next, we provide an outline of the constitutive models used for the granite. Next, we address the calibration the models. Finally, a summary of the modelling approaches is presented.

### 8.3.1 Physical phenomena considered

For comparison purposes, we summarise the main features of the models used by the various teams. Additional information concerning constitutive details for the granite will be given in the next section.

**BGR:** Three submodels have been used, a 2D axisymmetric (about the tunnel axis) TH submodel, a 2D plain strain “cut” (tunnel cross section through heater 2) TM submodel and a 2D “cut” (tunnel cross section through heater 2) TH submodel. The 2D axisymmetric TH submodel considered unsaturated liquid water flow and heat flow, and the zone modelled included granite rock, lamprophyre, EDZ, bentonite buffer, concrete plug, steel liner and heaters. The “cut” TM submodel considered the deformations of the materials and the heat flow, whereas the “cut” TH submodel considered the heat flow and the liquid water flow and, in both “cut” submodels, the zone modelled included only the granite. These two “cut” submodels were derived from a THM model that can consider the deformations of the materials, the flows of liquid water and heat in a coupled way, but as it is still in a test phase, and some of the aforementioned couplings were not complete, it was used considering only the TM and the TH couplings. In order to overcome the fact that neither the bentonite buffer nor the heaters are modelled in these two “cut” submodels, the experimentally measured pressure on the tunnel wall due to the swelling of the bentonite was applied as a boundary condition in the “cut” TM submodel, whereas the temperature at the tunnel wall provided by the axisymmetric TH submodel was applied as a boundary condition in the “cut” TH submodel. Within this model setup, the axisymmetric HM submodel provided the temperatures, the “cut” TH submodel provided the pore water pressures and the “cut” TM provided the stresses and the displacements.

**CNS:** The 3D model used was a fully coupled THM model with axisymmetric geometry (in fact, 1/4 of the full axisymmetric geometry). The model included deformation, liquid water flow, water vapour flow and heat flow. Phase changes between liquid water and water vapour as well as the thermal dilation of both the solid skeleton and the liquid water were also considered. The flow of air was not explicitly considered, as it was assumed that the gas pressure remained constant. The zone modelled included granite, lamprophyres, bentonite buffer and heaters. Concerning the state at the beginning of the test, the isothermal saturation of the bentonite buffer during the 180 days was taken into account. This model is essentially the same model that was used in Part B, but the size of the modelled zone was increased (the radius of the cylindrical zone modelled was increased from 11 m to 50 m) and the hydraulic boundary conditions were changed in order to match better the results obtained in Part A.

**DOE:** The 3D model used was made of two submodels, a TH submodel (multiphase, multicomponent fluid flow and heat transfer in porous media) and a TM submodel (mechanical and thermal deformations). These two submodels were only coupled in one direction, from the TH submodel to the TM submodel, as it was not possible to solve certain stability problems encountered when they were coupled in both directions. The TH submodel considered the flows of liquid water, water vapour and heat, and the zone modelled included the granite, the lamprophyres and the bentonite. In this submodel, phase changes between liquid water and water vapour were allowed, as well as the thermal dilation of the liquid water. The TM submodel considered the mechanical deformations, whereas deformations due to temperature and suction variations were taken into account as a variation of an artificial temperature, and the zone modelled included the granite, the lamprophyres, the bentonite and the heaters. In this submodel,

the gas phase was assumed to have a constant value. Concerning the state at the beginning of the test, the isothermal resaturation of the bentonite buffer during 192 day was taken into account.

**IPS:** The 2D axisymmetric model used was made of three submodels, a T-submodel (heat flow), a H-submodel (liquid water flow) and a M-submodel (mechanical deformations). These three submodels were fully coupled by use of a staggering technique. The model considered mechanical deformations and the flows of liquid water and heat, and the zone modelled included the bentonite buffer and the granite. The gas phase was not explicitly taken into account, whereby a constant pressure was assumed. The flow of water vapour was not considered and phase changes between liquid water and water vapour were not allowed. The granite was assumed to remain saturated. The thermal dilation of the liquid water and the thermal dilation of the solid skeleton were taken into account. Concerning the state at the beginning of the test, it was assumed that the isothermal resaturation of the bentonite buffer had reached equilibrium when the heaters were switched on.

**JNC:** The 3D model (in fact, 1/2 of the full geometry) used was a fully coupled HM model. Although the code used allows solving coupled THM problems, the modelling team did not consider the mechanical part in the present case, whereby all materials were assumed to be rigid. The model included liquid water flow, water vapour flow and heat flow, and the zone modelled included host rock, bentonite, concrete plug and heaters. Phase changes between liquid water and water vapour were allowed. The thermal dilation of the liquid water and the thermal dilation of the solid skeleton were taken into account. Concerning the gas phase, a constant gas pressure was assumed. The isothermal resaturation of the bentonite buffer prior to the operation of the heaters was not explicitly modelled.

**SKB:** The 3D model used was made of two submodels, a T submodel (heat flow) and a HM (mechanical deformations and water flow) submodel. These two submodels were coupled by use of a staggering technique. The T submodel considered the heat flow, and the zone modelled included the granite, the lamprophyres, the concrete plug and the bentonite. The HM submodel considered the mechanical deformation of the materials and the flows of liquid water, water vapour and heat, and the zone modelled included the bentonite buffer the granite, the lamprophyres, the concrete plug and the bentonite. In this submodel, phase changes between liquid water and water vapour were allowed, but the gas phase was not modelled, whereby its pressure was considered to be constant. The thermal dilation of the liquid water and the thermal dilation of the solid skeleton were taken into account. The isothermal resaturation of the bentonite buffer prior to the operation of the heaters was not explicitly modelled. Finally, due to the ability of the code to connect structures with different element mesh and element density, the modelled zone was large enough (600 m × 150 m × 300 m) so as to reach natural boundaries but the mesh was much finer near the FEBEX tunnel.

**SKI:** The 3D model used was a fully coupled THM model. The model considered the mechanical deformations of the materials and the flows of liquid water, water vapour and heat, and the zone modelled included granite, lamprophyres, bentonite buffer and heaters. Phase changes between liquid water and water vapour were allowed. The gas phase was not explicitly considered, whereby its pressure was taken to be constant. A noteworthy feature was the detailed modelling of the isothermal saturation of the bentonite previous to the switching on of the heaters, whereby two phases were considered. The first phase corresponded to the buffer installation (4 months) and hydration proceeded only through the lower part of the tunnel surface. The second phase

corresponded to the buffer hydration after the complete installation of the buffer (4.7 months) and hydration proceeded through the entire tunnel surface.

In order to give a quick overview, Table 8.1 summarises the main features of the models considered by the various teams.

*Table 8.1: Main features of the models used.*

Team	couplings	heat flow	rock th. dil.	wat. th. dil.	wat. flow
ANG	–	–	–	–	–
BGR	TH→(TM, TH)	X	X		X
CNS	THM	X	X	X	X
DOE	TH→TM	X	X	X	X
IPS	THM	X	X	X	X
JNC	TH	X		X	X
SKB	THM	X	X	X	X
SKI	THM	X	X	X	X

### 8.3.2 Constitutive models for the granite

Since the main concern here is the granite, in what follows, the constitutive equations considered by each modelling team pertinent to the granite are briefly summarised, whereby the hydraulic, thermal and mechanical aspects are addressed.

**BGR:** The constitutive equations considered for the granite are: (1) Hydraulic: Darcy’s law with a constant permeability; (2) Thermal: Fourier’s law with a constant thermal conductivity, constant thermal dilation of the rock skeleton and no thermal dilation of water; (3) Mechanical: linear thermoelasticity (Hooke’s law) for Terzaghi’s effective stress. In addition, it has been assumed that the granite remains saturated.

**CNS:** The constitutive equations considered for the granite are: (1) Hydraulic: van Genuchten’s law for the water retention curve, extension of Darcy’s law to unsaturated states with a constant saturated permeability and a van Genuchten’s law for the relative permeability to water; (2) Thermal: Fourier’s law with a constant thermal conductivity, constant thermal dilation of rock and constant thermal dilation of water; (3) Mechanical: linear thermoelasticity (Hooke’s law) for Bishop’s effective stress.

**DOE:** The constitutive equations considered for the granite are: (1) Hydraulic: van Genuchten’s water retention curve and an extension of Darcy’s law to unsaturated states with a constant saturated permeability and a van Genuchten’s relative permeability for liquid water; (2) Thermal: Fourier’s law with a constant thermal conductivity, a constant thermal dilation of rock and thermal dilation of water; (3) Mechanical: linear elastic. The change of the mechanical part of the model from the CJM (Compliant Joint Model) model used in Part A to the present linear elastic model is justified by the negligible effect of modelling the fractures and the high computational cost involved in the calculations using the CJM.

**IPS:** The constitutive equations considered for the granite are: (1) Hydraulic: Darcy’s law with a constant saturated permeability (the granite was assumed to remain saturated); (2) Thermal: Fourier’s law with a constant thermal conductivity, constant thermal dilation of water and thermal constant dilation of rock; (3) Mechanical: Biot’s linear poroelasticity with the Biot coefficient set to one (Terzaghi’s assumption).

**JNC:** The constitutive equations considered for the granite are: (1) Hydraulic: van Genuchten's water retention curve, the liquid water flow is governed by an extension of Darcy's law to unsaturated states with a saturated permeability depending on dry density and a van Genuchten's relative permeability and the water vapour diffusion was driven by temperature gradients with a constant thermal diffusivity; and (2) Thermal: Fourier's law with a thermal conductivity depending on the degree of saturation, constant thermal dilation of water and thermal constant dilation of rock; (3) Mechanical: rigid.

**SKB:** The constitutive equations considered for the granite are: (1) Hydraulic: the liquid water flow was governed by Darcy's law with a constant permeability; (2) Thermal: Fourier's law with a constant thermal conductivity, constant thermal dilation of water and thermal constant dilation of rock; (3) Mechanical: thermoporoelasticity based on Bishop's effective stress. Similar constitutive equations were used for the lamprophyres.

**SKI:** The constitutive equations considered for the granite are: (1) Hydraulic: van Genuchten's water retention curve, the liquid water flow was governed by an extension of Darcy's law to unsaturated states with a constant anisotropic saturated permeability and the diffusive water vapour flow was governed by Fick's law; (2) Thermal: Fourier's law with a constant thermal conductivity, constant thermal dilation of water and thermal constant dilation of rock; (3) Mechanical: thermoporoelasticity based on Bishop's effective stress. Similar constitutive equations were employed for the lamprophyres.

### 8.3.3 Model calibration

We will provide only a brief outline of the calibration procedures that have been used by each modelling team.

**BGR:** Some model functions and model parameters have been taken from the case definition, and others from the specialised literature and the author's experience. In order to assess the influence of the Young's modulus and the thermal dilation coefficient of the rock skeleton, some sensitivity analyses have been carried out.

**CNS:** As the model used was essentially the model used in Part B, no further calibrations were made. However, the hydraulic boundary conditions were modified in order to approximate the pore water distributions obtained in Part A.

**DOE:** As the model used was a simplification of the models used in Part A (elastic rock instead of CJM) and Part B, no further calibrations were carried out.

**IPS:** The model used was the same as the model used in Part B, except for being 2D axisymmetric instead of 1D plain strain axisymmetric. Therefore, no additional calibrations were carried out.

**JNC:** As the model used was the same as the model used in Part B, no additional calibrations were carried out.

**SKB:** As the model used was a combination of the models for Part A (rock) and Part B (bentonite), the calibrations carried out in Part A for the rock (granite and lamprophyres) and in Part B for the bentonite were used in the present model. It was however, checked that results obtained were consistent with the results obtained in Parts A and B.

**SKI:** Since the model used was essentially the same as the model used in Part A and in Part B, no further calibrations were needed.

### 8.3.4 Summary of the modelling approaches

In order to facilitate the understanding of the results provided by the teams, this section includes a summary with the main features of the approaches followed by the modelling teams. In as much as possible, a common structure has been used in all these summaries (modelling hypotheses, equations solved and programs used). Besides some general features, these summaries intend to address the aspects that are believed to be relevant to the present case.

#### 8.3.4.1 Approach followed by BGR

##### a) General modelling features

- Dimensions: 2D axisymmetric for axisym TH; 2D cross section for “cut” TM , “cut” TH
- Couplings: axisym TH → “cut” TM and “cut” TH
- Materials: axisym TH: bentonite, rock, lamprophyre dykes, concrete plug, heater. “cut” TM and “cut” TH: granite
- Load. history: axisym TH: heating (33 months).

##### b) Physical phenomena considered

- Deformation (rock).
- Flows of liquid water (bentonite and rock) and air (bentonite).
- Flow of heat (bentonite and rock).
- Thermal dilation (rock).

##### c) Main simplifying assumptions

- Thermal equilibrium.
- Granite remains saturated.
- No thermal dilation of water.
- Internal energy convective terms neglected in the balance of energy equation.
- Constant specific heat and conductivity in the balance of energy equation.

##### d) Equations solved

- Water mass balance + saturated (rock) / unsaturated (bentonite) Darcy flow.
- Air mass balance + unsaturated Darcy flow (bentonite)
- Balance of momentum (rock).
- Balance of energy + Fourier’s heat conduction law.

##### e) Main features of the granite model

- Mechanical: linear thermoelasticity (Hooke’s law) for Terzaghi’s effective stress.
- Hydraulic: wat. perm.: constant.
- Thermal: therm. conduct.: constant.  
rock therm. dil.: constant.  
wat. therm. dil.: zero

f) Programs used

- RF/RM (finite element method code developed by a research group: University of Tübingen, University of Hannover and Leibniz Institute for Applied Sciences).

g) Remarks

- The experimentally measured radial stresses have been applied to the tunnel wall.

**8.3.4.2 Approach followed by CNS**

a) General modelling features

- Dimensions: 3D analysis with axisymmetric geometry (1/4 of the full geometry).
- Couplings: full THM.
- Materials: bentonite, surrounding rock, lamprophyre dykes, concrete plug, heater.
- Load. history: buffer hydration (6 moths) and heating (33 months).

b) Physical phenomena considered

- Mechanical deformation.
- Flows of liquid water and water vapour.
- Phase change liquid water  $\leftrightarrow$  water vapour.
- Flow of heat.
- Thermal dilation (rock and water).

c) Main simplifying assumptions

- Constant gas pressure.
- Mechanical power neglected in the balance of energy.
- Thermal equilibrium.
- Vapour flux is induced by temperature gradients.
- Internal energy convective terms neglected in the balance of energy equation.

d) Equations solved

- Balance of momentum for the porous medium.
- Water mass balance + unsaturated Darcy flow + vapour flux.
- Balance of energy + Fourier's heat conduction law.

e) Main features of the granite model

- Mechanical: linear thermoelasticity (Hooke's law) for Bishop's effective stress.
- Hydraulic: retention curve: van Genuchten (case def.).  
sat. wat. perm.: constant.  
rel. wat. perm.: van Genuchten (case def.).  
therm. vap. diff.: constant
- Thermal: therm. conduct.: depending linearly on Sr (references)  
rock therm dil.: constant.  
wat. therm. dil.: constant.

#### f) Programs used

- FRACON (finite element method code developed by Canadian Atomic Energy Control Board and McGill University).

### **8.3.4.3 Approach followed by DOE**

#### a) General modelling features

- Dimensions: 3D TH and TM analyses.
- Couplings: one-way TH → TM (in fact, TH → M).
- Materials: TH: bentonite, surrounding rock, lamprophyre dykes, heater.  
TM: bentonite, surrounding rock, lamprophyre dykes, heater.
- Load. history: buffer hydration (192 days) and heating (33 months).

#### Physical phenomena considered

- Mechanical deformation.
- Flows of liquid water and water vapour.
- Phase change liquid water ↔ water vapour.
- Flow of heat.
- Thermal dilation (rock, bentonite and water).

#### Main simplifying assumptions

- Constant gas pressure.
- Thermal equilibrium.
- No water vapour pressure lowering in the bentonite ( $S_r = 1$  whenever water is present)

#### Equations solved

- Balance of momentum for the porous medium.
- Water mass balance + unsaturated Darcy flow + vapour flux.
- Balance of energy + Fourier's heat conduction law.

#### Main features of the granite model

- Mechanical: linear elastic
- Hydraulic: retention curve: van Genuchten (case def.).  
sat. wat. perm.: constant.  
rel. wat. perm.: van Genuchten (case def.).  
therm. vap. diff.: constant
- Thermal: therm. conduct.: constant  
rock therm dil.: constant.  
wat. therm. dil.:

#### Programs used

- TH calculations. THOUGH2 (commercial finite difference code).
- TM calculations: JAS3D (finite element code developed at Sandia National Laboratories)

#### **8.3.4.4 Approach followed by IPS**

##### a) General modelling features

- Dimensions: 2D axisymmetric analysis.
- Couplings: full THM via staggering.
- Materials: bentonite and surrounding rock.
- Load. history: equilibrium buffer hydration, heating (33 months).

##### b) Physical phenomena considered

- Mechanical deformation.
- Flow of liquid water.
- Flow of heat.
- Thermal dilation (rock, bentonite and water).

##### c) Main simplifying assumptions

- The granite remains saturated.
- Constant gas pressure.
- Thermal equilibrium.
- Water vapour flux neglected.
- No phase change liquid water ↔ water vapour.
- Dry air is not taken into account in the balance of energy.

##### d) Equations solved

- Balance of momentum for the porous medium.
- Water mass balance + unsaturated (bentonite) / saturated (rock) Darcy flow
- Balance of energy + Fourier's heat conduction law.

##### e) Main features of the granite model

- Mechanical: Biot's linear thermoporoelasticity with Terzaghi's assumption
- Hydraulic: sat. wat. perm.: constant
- Thermal: therm. conduct.: constant.  
rock therm dil.: constant  
wat. therm. dil.: constant

##### f) Programs used

- T calculations. CHEF (own finite element code).
- H calculations: HYDREF (own finite element code).
- M calculations: VIPLEF (own finite element code).

#### **8.3.4.5 Approach followed by JNC**

##### a) General modelling features

- Dimensions: 3D (1/2 of the full geometry).
- Couplings: full TH.
- Materials: bentonite, surrounding rock, lamprophyre dykes?, concrete plug?, heater?.
- Load. history: heating (33 months).

b) Physical phenomena considered

- Flows of liquid water and water vapour.
- Phase change liquid water ↔ water vapour.
- Flow of heat.
- Thermal dilation (water).

c) Main simplifying assumptions

- Materials do not deform.
- Air is not taken into account (constant gas pressure).
- Thermal equilibrium.
- Vapour flux is induced by temperature gradients.

d) Equations solved

- Water mass balance + unsaturated Darcy flow + vapour flux.
- Balance of energy + Fourier's heat conduction law.

e) Main features of the granite model

- Mechanical: rigid.
- Hydraulic: retention curve: modified van Genuchten (case def.).  
sat. wat. perm.: constant  
rel. wat. perm.: van Genuchten (case def.)  
therm. vap. diff.: constant
- Thermal: therm. conduct.: constant.  
rock therm dil.: zero.  
wat. therm. dil.: constant

f) Programs used

- THAMES3D (finite element method code developed by Kyoto University).

**8.3.4.6 Approach followed by SKB**

a) General modelling features

- Dimensions: 3D T and HM analyses.
- Couplings: full T↔HM via staggering.
- Materials: T: bentonite, rock, lamprophyres, concrete plug, heaters.  
HM: bentonite, rock, lamprophyres, concrete plug, heaters.
- Load. history: heating (33 months).

b) Physical phenomena considered

- Mechanical deformation.
- Flow of liquid water
- Flow of heat.
- Thermal dilation (rock, bentonite and water).

c) Main simplifying assumptions

- Thermal equilibrium.
- Mechanical power neglected in the balance of energy.

#### d) Equations solved

- Balance of momentum for the porous medium.
- Water mass balance + Darcy flow.
- Balance of energy + Fourier's heat conduction law.

#### e) Main features of the granite model

- Mechanical: thermoporoelasticity based on Terzaghi's effective stress.
- Hydraulic: sat. wat. perm.: constant and anisotropic.  
thermal: therm. conduct.: constant.  
rock therm dil.: constant.  
wat. therm. dil.: constant.

#### f) Programs used

- ABAQUS (commercial finite element method code) with some user-defined routines.

### **8.3.4.7 Approach followed by SKI**

#### a) General modelling features

- Dimensions: 3D (1/2 of the full geometry, limited by a vertical plane).
- Couplings: full THM.
- Materials: bentonite, surrounding rock, lamprophyre dykes, concrete plug, heater.
- Load. history: buffer installation (4 months), buffer hydration (4.7 months) and heating (33 months).

#### b) Physical phenomena considered

- Mechanical deformation.
- Flows of liquid water and water vapour.
- Flow of heat.
- Phase change liquid water ↔ water vapour.
- Thermal dilation (rock, bentonite and water).

#### c) Main simplifying assumptions

- Constant gas pressure.
- Mechanical power neglected in the balance of energy.
- Thermal equilibrium.
- Phase change liquid water ↔ water vapour equilibrium.

#### d) Equations solved

- Balance of momentum for the porous medium.
- Water mass balance + unsaturated Darcy flow + vapour Fick flow.
- Balance of energy + Fourier's heat conduction law.

#### e) Main features of the granite model

- Mechanical: linear thermoporoelasticity based on Bishop's effective stress.
- Hydraulic: retention curve: van Genuchten (case def.).

- sat. wat. perm.: constant and anisotropic.
- rel. wat. perm.:
- vap. Fick diff.:
- Thermal: therm. conduct.: constant.
- rock therm dil.: constant.
- wat. therm. dil.: constant.

#### f) Programs used

- ROCMAS (finite element method code developed at Lawrence Berkeley National Laboratory).

## 8.4 Relevant physical phenomena

Previous modelling work of the FEBEX in situ test carried out at the UPC (see, for instance, Gens et al., 1998a) allowed an understanding of the physical phenomena involved in the thermo-hydro-mechanical behaviour of the surrounding rock massif. This background, together with the teams' reports, was used in order to understand the success of the numerical predictions provided by the teams. In this regard, the discussions among the teams and the coordinator during the project have been very useful.

This section is structured as follows. First some features of the observed experimental data will be presented. Then, based on previous modelling work carried out at the UPC, the main processes taking place in the host rock will be outlined. Finally, a summary of the physical phenomena that are considered to be relevant to reproduce the observed behavior will be presented. These phenomena will be used in the next section in order to understand the success of the numerical predictions provided by the teams.

### 8.4.1 Features of the experimental data

Looking at the experimental data, a number of interesting features may be noticed. We will divide their presentation according to the variables requested in the case definition.

- **Temperature.** Experimental measurements of temperature exhibit a monotonously increasing pattern. Temperatures increase faster during the first two months after which they slowly approach asymptotic values.
- **Pore water pressure.** Measured pore water pressures near the tunnel wall increase slowly in a monotonous way from a value close to 0.5 MPa to a value around 0.7 MPa. Essentially, no marked transients in pore water pressures are observed. However, the pressure evolution of the water used to inflate the packers dividing the instrumented boreholes into intervals exhibits much larger variations, reaching maximum values close to 5 MPa, as shown in Figure 8.1.
- **Total stresses.** The evolutions of all the three measured total stress components are characterised by an initial fast increase until a peak is reached at about 100 days, followed by a slow slight decrease and an even slower increase, without, however, approaching any asymptotic value during the period of 1000 days. Measured total stresses decrease significantly with the distance.

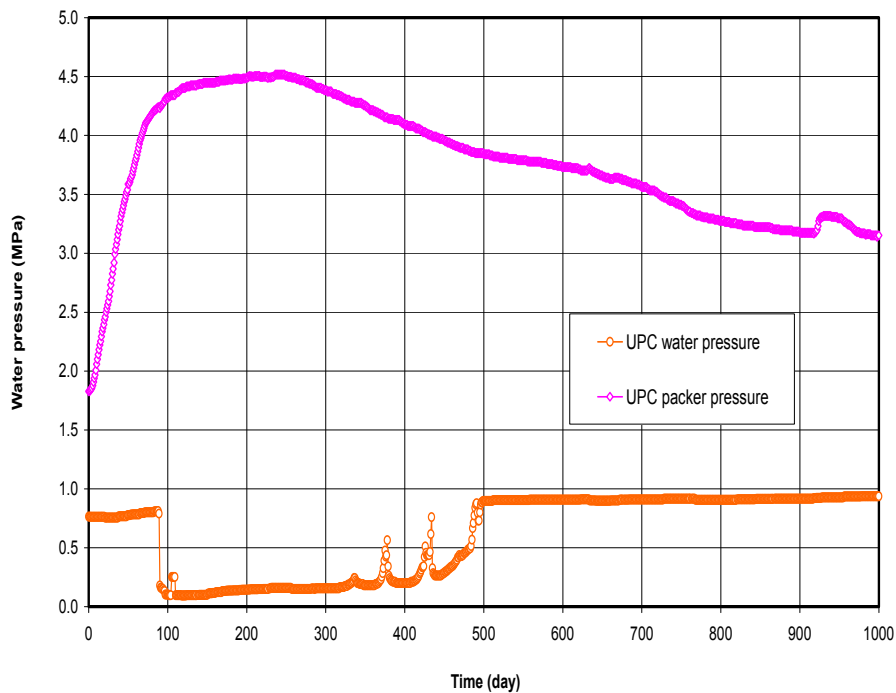


Figure 8.1: Measured evolutions of pressures at borehole SF21. Water pressure at the packed off interval closest to the tunnel (centre at  $r = 3.03$  m) and inflation pressure of the packer closest to the tunnel (centre at  $r = 1.86$  m).

- **Radial displacements.** Measured maximum radial displacements were in the range of about 100 microns. Their evolutions exhibit an initial fast increase followed by a very small subsequent increase. The magnitude of these displacements and their evolutions cast doubts on their accuracy.

#### 8.4.2 Main processes taking place in the bentonite barrier

Based on previous modelling work of the FEBEX in situ test, the main processes taking place on the rock surrounding the FEBEX test will be briefly presented. It must be borne in mind that these processes are deemed to be relevant to the present case, but in other (apparently) similar cases, it may well happen that some of these processes relevant to the present case become irrelevant, while other processes irrelevant to the present case become relevant. Furthermore, since only the first 1000 days of operation of the FEBEX in situ test are considered, it may also occur that some processes irrelevant during that initial period become important at later stages.

As in the case of the observed features of the experimental data, the presentation will be divided according to the variables requested in the case definition.

- **Temperature.** Since heat flow due to convection and diffusion are due to transport by the comparatively slow fluid motions, but temperatures approach rather fast a steady state, it is concluded that heat flow essentially by conduction. Therefore, reliable values for the thermal conductivity are mandatory in order to reproduce the observed temperature patterns.

- **Pore water pressure.** Due to the different dilation of the pore water and the rock skeleton, a transient increase in temperature in a saturated porous medium induces a transient increase and a subsequent decrease in pore water pressure. The magnitude of the increase of the pore water pressure increases with the rate of temperature increase, the porosity and the rock stiffness and decreases with the rock permeability. The rate of dissipation of the increase of pore water pressure increases with the rock permeability. As no clear transients of pore water pressure were recorded, this indicates comparatively high values of the rock permeability. This view is supported by the observed evolution of the pressure of the water used to inflate the packers dividing the instrumented boreholes into intervals, exhibiting essentially an undrained behaviour. Therefore a hydro-mechanical coupling is warranted only if some insight on the aforementioned transients is desired.
- **Total stress.** The variation of the total stresses is the sum of the variation of the effective stresses (due to the mechanical deformation of the rock) and the variation of the pore water pressure (due to the thermal dilation of the water and subsequent dissipation of the induced increases of pore water pressure). The stresses induced in the rock are due to the thermal dilation of the rock and, to a lesser extent, to the swelling pressure transmitted by the bentonite buffer. On the other hand, the peaks observed in the evolutions of the total stress components may be explained by the corresponding pore water pressure evolutions. Therefore, at least a T→HM model is required in order to reproduce the observed behaviour, whereby the T model must consider heat flow and rock and water dilation.
- **Radial displacement.** The variation of radial displacements is a consequence of the variation of the temperature and of the effective stresses. Therefore, the arguments above indicate the need of at least a T→HM model. However, due to the comparatively high stiffness of the rock surrounding the FEBEX test, displacements will be very small and difficult to measure accurately.

It is interesting at this point to compare the evolutions of the water pressure at the packed off intervals with the evolutions of the inflation pressure of the. Figure 1 shows such a comparison at borehole SF21, whereby the packed off interval closest to the tunnel and the packer closest to the tunnel are considered. For the packer, the initially recorded pressure is related to the pressure applied to seal the borehole. Afterwards, the circuit is closed in order to maintain constant volume conditions. The substantial increase in pressure observed is most probably due to the thermal induced dilation of the water inside the packer system. Presumably, the deformation of the packer and measuring system and/or minor leaks lead to a progressive decay afterwards. The relevant point here is, as shown in Figure 8.1, that this type of behaviour was not observed in the water pressure measuring intervals in direct connection to the granitic rock.

A transient increase in temperature of a porous medium such as a saturated rock induces a transient increase and subsequent decrease in pore water pressure, which depends on the rate of temperature increase, the rock permeability, the rock porosity, the rock stiffness and the geometry (drainage conditions). Water pressure increases because water dilates more than the rock skeleton. In parallel, a drainage process reduces excess pore pressures towards zero. The higher the porosity, the higher peak pore water pressure is observed. The lower the permeability and the higher the stiffness of the rock, the higher the pore water pressure peak and the slower the subsequent dissipation. The fact that no transient excess pore water pressures were detected in the rock is probably

due to the relatively high permeability of the rock. Excess pore water pressures dissipate immediately after they are induced. In addition, recorded water pressures are average values over the measuring interval. This effect contributes also to reduce the excess pore water pressures. The different conditions of the packer system (a “high” porosity and a rigid confinement) explain the completely different behaviour recorded.

A calculation of the evolution of effective mean stress and the octahedral shear stress in borehole SG” at a radial distance  $r = 3$  m has been made. Pore pressures were approximated by data collected in neighbouring boreholes. It was also assumed that normal stresses on the three normal planes are principal stresses. The results are given in Table 8.2 below.

*Table 8.2: Evolutions of increments of mean effective stress  $\Delta p'$ , octahedral shear stress  $\Delta \tau_{oct}$  and maximum shear stress  $\Delta \tau_{max}$  in Borehole SG2 at  $r \approx 3.0$  m.*

Time [day]	$\Delta p'$ [MPa]	$\Delta \tau_{oct}$ [MPa]	$\Delta \tau_{max}$ [MPa]
0	0.00	0.00	0.00
100	2.56	0.82	1.00
300	1.96	0.37	0.40
700	2.26	0.53	0.65
1000	2.80	0.53	0.65

Note that the values given are increments over the initial state of stress once the FEBEX tunnel was open. They represent therefore the combined effect of temperature effects (the dominant phenomenon), the generation and dissipation of pore pressures and the swelling pressure effects. At radial distance of 3 m, the increments of mean effective stress dominate. Incremental shear stresses tend to be a fraction of the incremental mean stresses. The maximum difference of effective normal stresses is slightly higher, as shown also in the same Table. Given the expected strength properties of the granite, the effective stress path corresponding to these values separates from the failure envelope. It is also interesting to note that the worst condition (in terms of proximity to a failure envelope) is met when total stresses reach a peak (at  $t = 100$  days approximately). At later times, mean effective stresses dominate.

From the previous considerations, it is apparent that at least a T→HM model is required, whereby the T-model must consider heat flow and rock and water dilation. However, the following simplifications were found to be pertinent to the FEBEX in situ test:

- **Homogeneous hydraulic conductivity of the rock.** Due to the comparatively high rock permeability, the characteristic time of heating was larger than the characteristic time of relaxation of pore water pressure. Consequently, the heterogeneous nature of the rock hydraulic conductivity features may be disregarded.
- **Negligible mechanical influence of the bentonite buffer.** On the one hand, the stress increments due to the swelling of the bentonite buffer are small when compared to the stress increments due to the heating action of the buffer on the rock. On the other hand, due to the relatively high stiffness of the host rock, the induced displacements are relatively small and very difficult to measure.

Therefore, for most practical purposes, a simplified constitutive model may be used for the bentonite.

### 8.4.3 Summary of the relevant physical phenomena

In order to explain the success of the Numerical Predictions provided by the various teams, the physical processes shown in Table 8.3 will be considered. As explained above, these physical processes have a direct influence on the evolutions and distributions of the variables requested in the case definition.

In the next section, the consideration of these physical phenomena in the different modelling approaches will be examined.

*Table 8.3: Selected physical phenomena relevant to Part C.*

Abbreviation	Physical phenomena
rock th. dil.	Thermal dilation of the rock skeleton
wat. th. dil.	Thermal dilation of water
HM	Hydro-Mechanical coupling

## 8.5 Comparison of experimental data with predictions

Teams have submitted two types of predictions: “blind” predictions and “latest” predictions. By “blind” predictions for Part C we mean the numerical predictions before the measured experimental data were disclosed to the teams. Not all the teams involved in a Part C of Task 1 submitted “blind” predictions and not all “blind” predictions provided all the required results. However, we believe that these “blind” predictions are very valuable, as they address the problem in the same way that it would be addressed in real instances.

In order to reflect both the “learning” and the “blind” aspects of Task 1, we have compared the experimental data with both the “latest” and the “blind” predictions. On the other hand, since the modelling approaches are based on the last version of the corresponding Modelling Reports, which are included as Appendixes, we will only make comments to the “latest” predictions.

Finally, in order to ease the comparison between “latest” and “blind” predictions, both the comparison plots with “latest” and the comparison plots with “blind” predictions have been arranged following exactly the same scheme. As explained later on, corresponding figures will have the same number and will only differ by a distinctive letter adjoined to the number.

### 8.5.1 Comparison with “latest” predictions

In this subsection, the “latest” numerical predictions by the teams will be compared with the corresponding measured values. From the set of all required numerical predictions, only a representative subset will be presented here in graphical form. Table 8.4 provides an overview of the consideration by the various models of the couplings and some key factors identified in the previous Section as relevant to the present case.

Table 8.4: Consideration of couplings and some key factors by the modelling teams.

Team	Couplings	Dimens	Rock th. Dil.	Wat. Th. Dil.	HM
ANG	–	–	–	–	
BGR	TH→(TM, TH)	2	X		X
CNS	THM	3	X	X	X
DOE	TH→TM	3	X	X	
IPS	THM	2	X	X	X
JNC	TH	3		X	X
SKB	THM	3	X	X	X
SKI	THM	3	X	X	X

Comments on comparisons plots are provided according to the variables whose evolutions and or distributions were requested in the case definition, namely: temperature, pore water pressure, total stress and radial displacement.

- **Temperature.** The comparison of the measured values with the predicted evolutions of temperature in Borehole SF21 at a radial distance of  $r = 1.20$  m (see Figure 8.2), shows that predictions by IPS, SKB and SKI are very good and predictions by BGR, CNS, DOE and JNC are good and the prediction by ANG deviates substantially from the measured values.
- **Pore water pressure.** The comparison of the measured values with the predicted evolutions of pore water pressure in Borehole SF21 at two points with radial distances  $r = 3.03$  m and  $r = 13.06$  m (see Figure 8.3), shows that none of the predictions approximates satisfactorily the measured evolutions of pore water pressure in both of the two points considered. Therefore, we will consider only what appear to be two general features of the measured evolutions of pore water pressures, namely the common sign of the rate of variation with time at the two considered points and the differences in the evolutions at the two considered points. Concerning the common sign of the rate of variation with time, measured pore water pressures increase monotonously with time. Predictions by CNS and DOE decrease monotonously with time, predictions by BGR and IPS essentially do not vary with time and predictions by JNC, SKB and SKI increase monotonously with time. Concerning the differences in the evolutions of pore water pressures at the two considered points, measured pore water pressure evolutions are different, predictions by ANG, BGR, CNS, DOE, IPS, SKB and SKI are different and predictions by CNS are essentially the same. The predictions by ANG exhibit a more complex behaviour, as there is an almost immediate large decrease followed by a monotonous increase with time.
- **Total stress.** The comparison of the measured values with the predicted evolutions of the total stress components in Borehole SG2 at a radial distance of  $r \approx 3.0$  m (see Figure 8.4), shows that, although none of the predictions approximates satisfactorily the measured evolutions, if we consider only the range of the measured values, predictions by BGR, SKB and SKI are good predictions, whereas predictions by ANG, CNS, DOE and IPS deviate substantially from the measured values. We remark that the observed shape of the total stress evolutions with the noteworthy feature of a peak at about 100 days, fails to be predicted by all modelling teams. Finally, let us mention that predictions by JNC are missing, since they did not include the deformations in their model.

- **Radial displacement.** The comparison of the measured values with the predicted evolutions of radial displacement in Borehole SI1 at a radial distance of  $r = 8.03$  m (see Figure 8.5), shows that the prediction by SKI is very good, the prediction by IPS is good, whereas predictions by ANG, BGR, DOE and SKB deviate substantially from the measured values.. However, if we consider only the first 100 days, predictions by ANG (disregarding the first few days), BGR, DOE and SKB are good. Finally, let us mention that predictions by JNC are missing, since they did not include the deformations in their model.

It should be mentioned that, as indicated in the previous Section, some modelling teams have used measured values (that should have been predicted by the model) in order to overcome some drawbacks of their model. Obviously, this is not possible in a “blind” prediction.

### 8.5.2 Comparison with “blind” predictions

In this subsection, the “blind” numerical predictions by the teams will be compared with the corresponding measured values, as shown in Figures 8.6 – 8.9. As indicated earlier, no specific comments will be made to these comparison plots with “blind” predictions because the various modelling approaches that have been presented in section 8.3 are based on the latest version of the teams’ reports.

Nevertheless, comparison plots will be arranged in the same way as were arranged the comparison plots for “latest” predictions. Seven teams submitted “blind” predictions for Part B, namely ANG, BGR, DOE, IPS, JNC, SKB and SKI. For clarity, figures have been split in two parts, whereby predictions by ANG, BGR and DOE against experimental data are shown in the first part of the figure and predictions by IPS, JNC, SKB and SKI against experimental are shown in the second part of the figure.

### 8.5.3 Discussion and conclusions

Coupled THM models are also required for this part of the study although the temperature increase plays a dominant role in the rock behavior.

Temperature distributions are well reproduced in general terms. In fact, some of the calculations are very precise, unlike the case of temperature prediction for the buffer. In the case of the (saturated) rock temperature is controlled by a constant parameter: the granite heat conduction coefficient. In the bentonite buffer, besides the effect of degree of saturation on conductivity and specific heat, other phenomena are at play: the heat transport associated with convective and diffusive flows of liquid water and vapour. This situation may explain te different performance of models in both cases.

Rock water pressures development integrates several separate phenomena: the modification of the hydrogeological regime in the vicinity of the tunnel due to the presence of the barrier, temperature effects and the influence of the suction of the bentonite. Temperature effects, in turn, depend on a number of rock properties: rock dilation coefficient, porosity, stiffness and permeability. The actual development of excess pore pressures are additionally controlled by the rate of temperature change and by the general drainage conditions in the area. Some of these effects go in opposite directions. For instance, if temperature-induced pore water pressure development is a dominant phenomenon, points closer to the experiment axis should be expected to

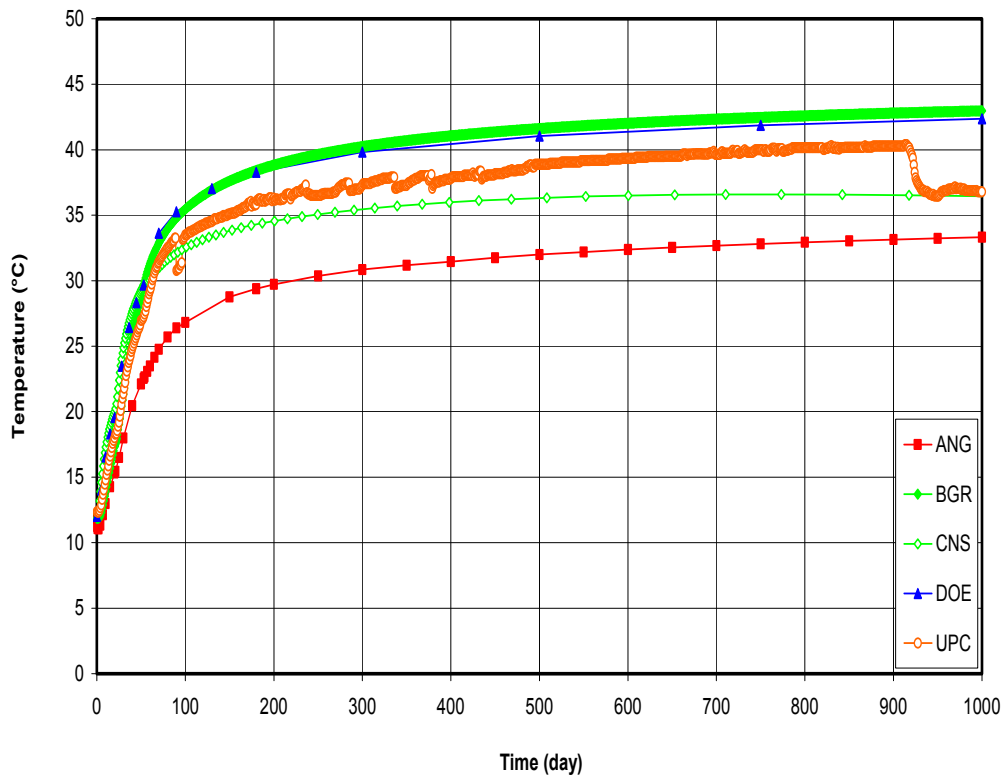


Figure 8.2a: Measured and predicted evolutions of temperature in borehole SF21 at point 1 ( $r = 1.20$  m).

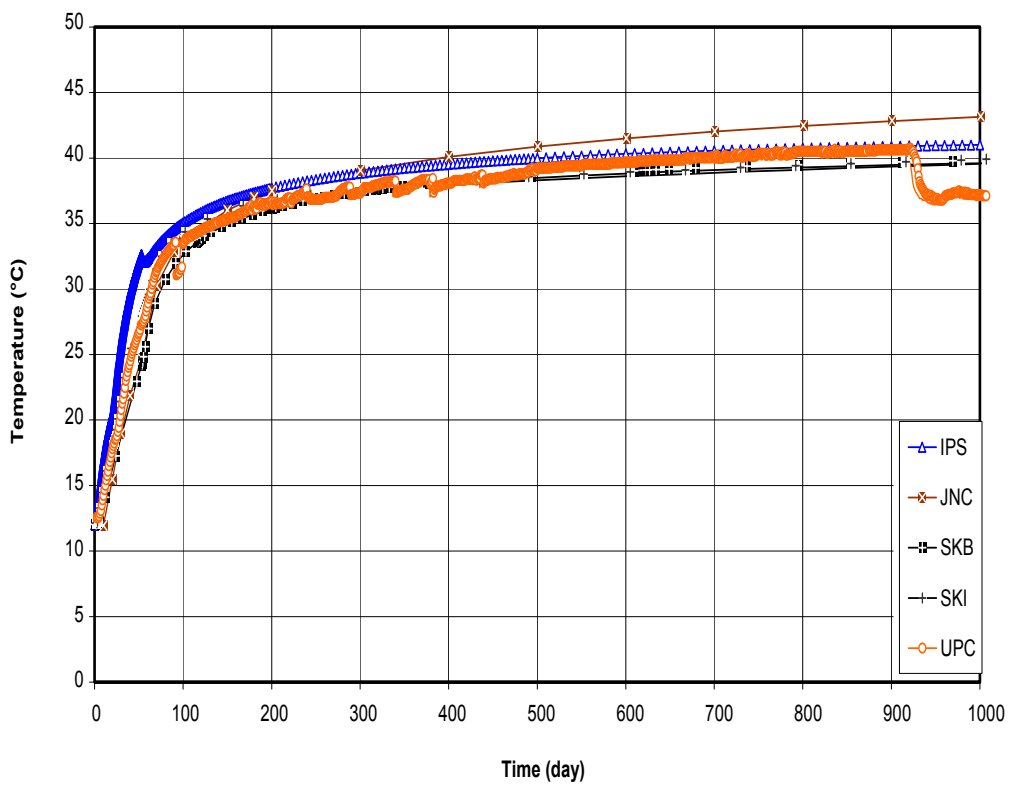


Figure 8.2b: Measured and predicted evolutions of temperature in borehole SF21 at point 1 ( $r = 1.20$  m).

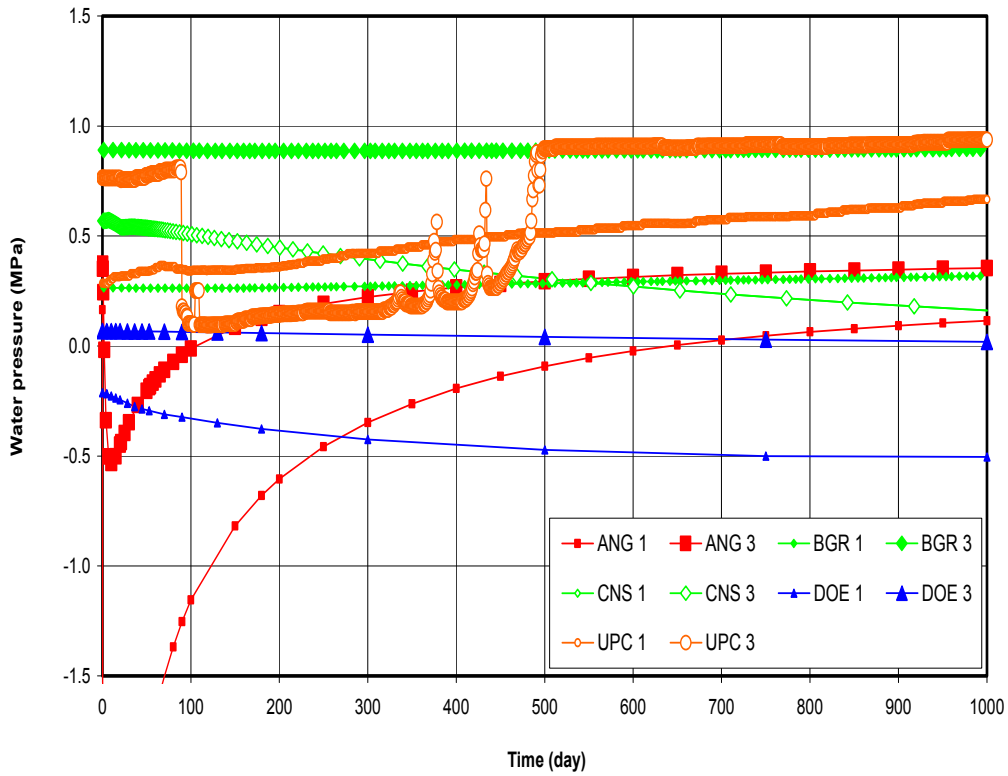


Figure 8.3a: Measured and predicted evolutions of water pressure in borehole SF21 at point 1 ( $r = 3.03$  m) and at point 3 (13.06) m.

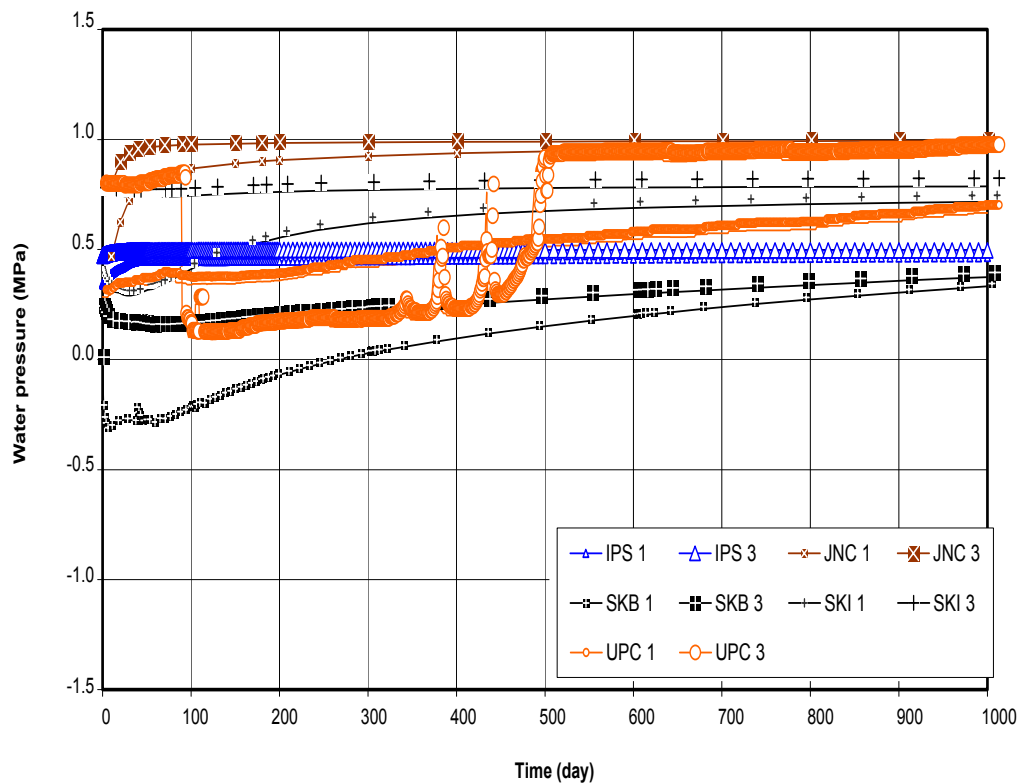


Figure 8.3b: Measured and predicted evolutions of water pressure in borehole SF21 at point 1 ( $r = 3.03$  m) and at point 3 (13.06) m.

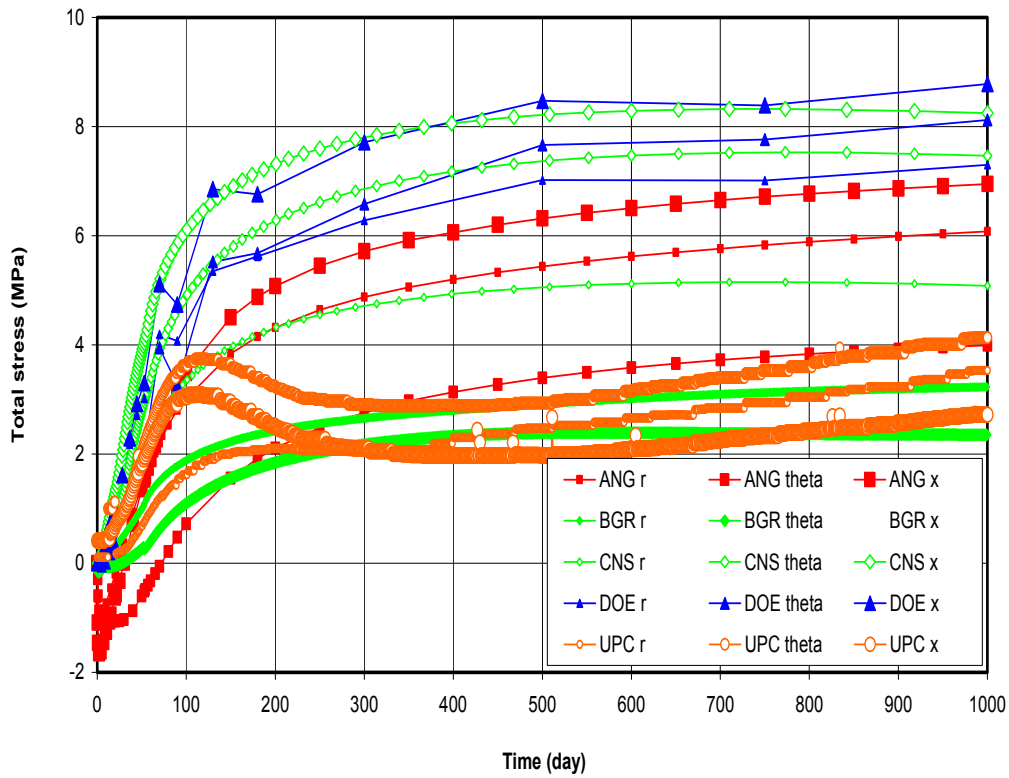


Figure 8.4a: Measured and predicted evolutions of total stress components in borehole SG2 at points 1, 2 and 3 ( $r \approx 3.0$  m).

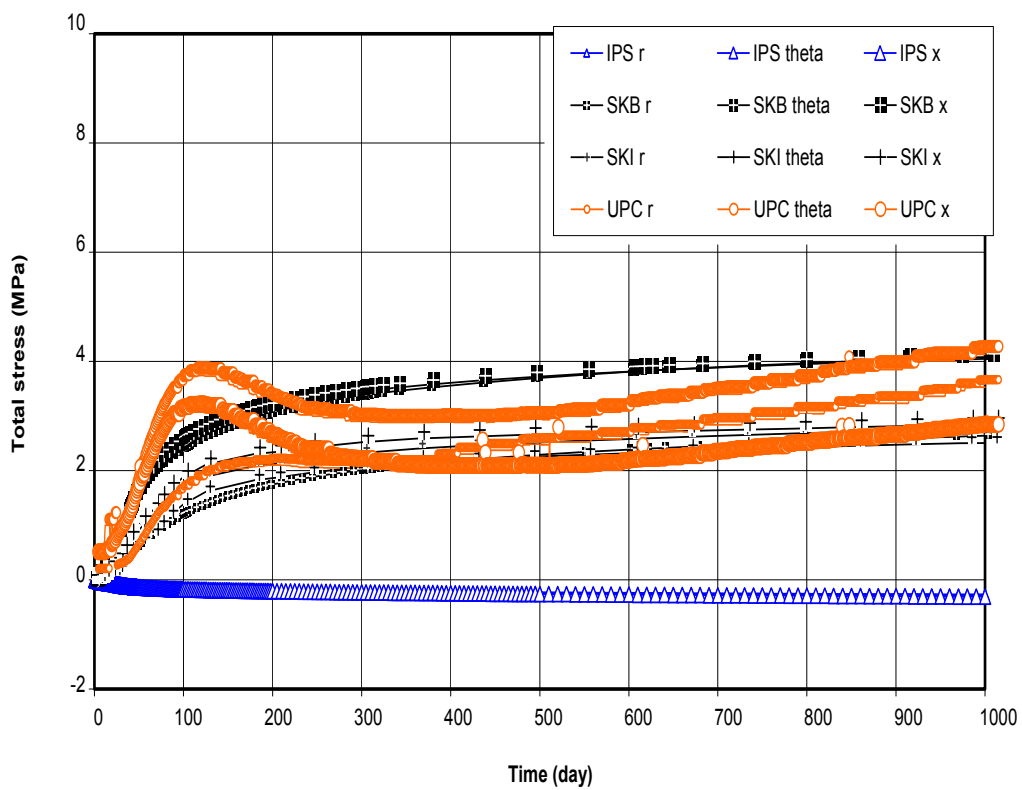


Figure 8.4b: Measured and predicted evolutions of total stress components in borehole SG2 at points 1, 2 and 3 ( $r \approx 3.0$  m).

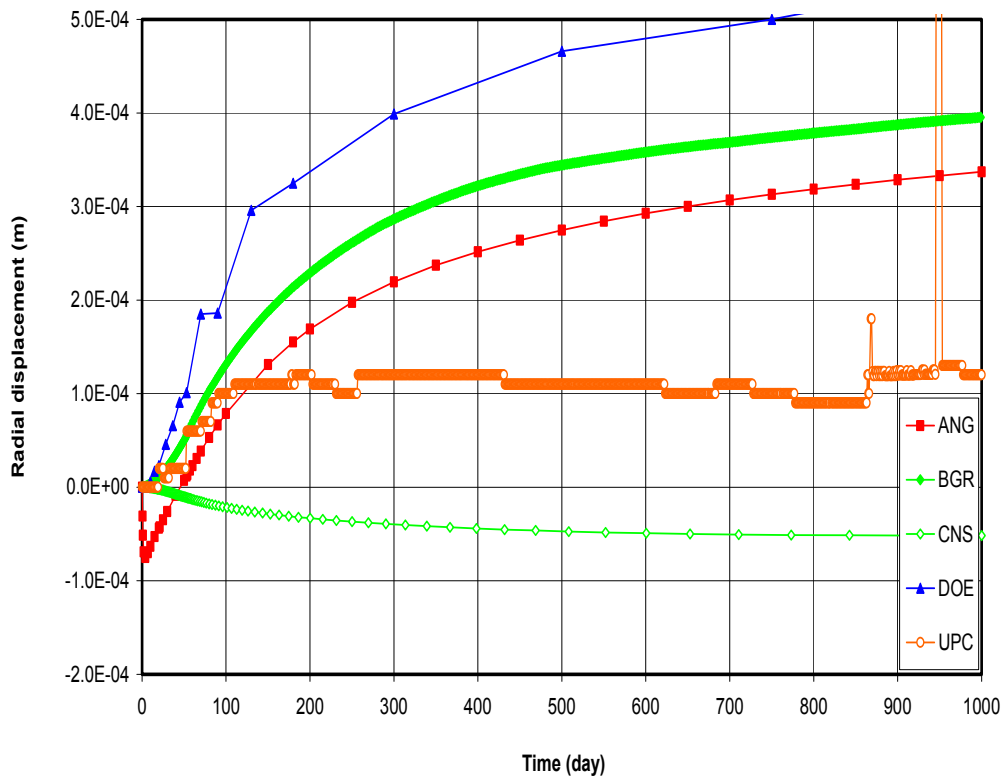


Figure 8.5a: Measured and predicted evolutions of radial displacements in borehole S11 at point 3 ( $r = 8.03$  m).

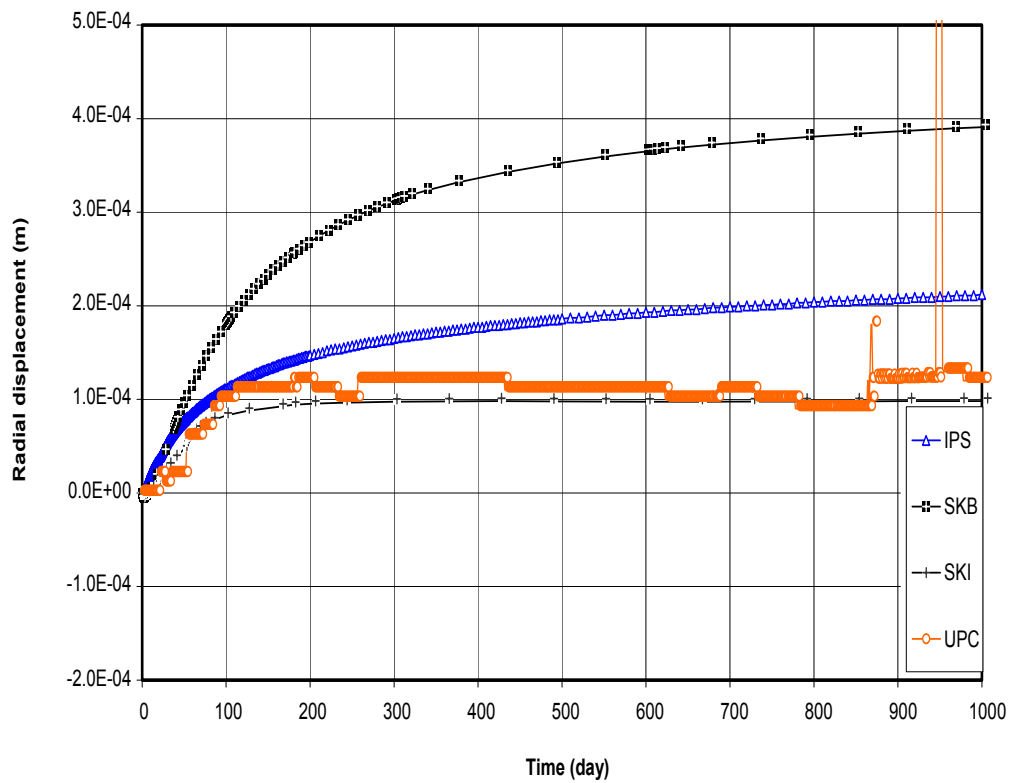


Figure 8.5b: Measured and predicted evolutions of radial displacements in borehole S11 at point 3 ( $r = 8.03$  m).

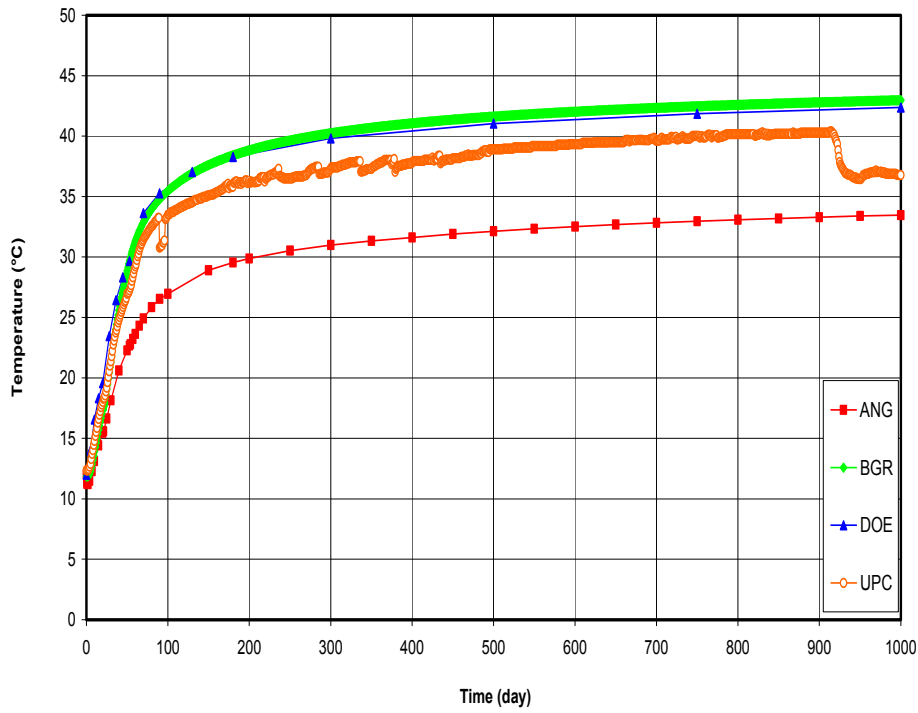


Figure 8.6a: Measured and predicted evolutions of temperature in borehole SF21 at point 1 ( $r = 1.20$  m).

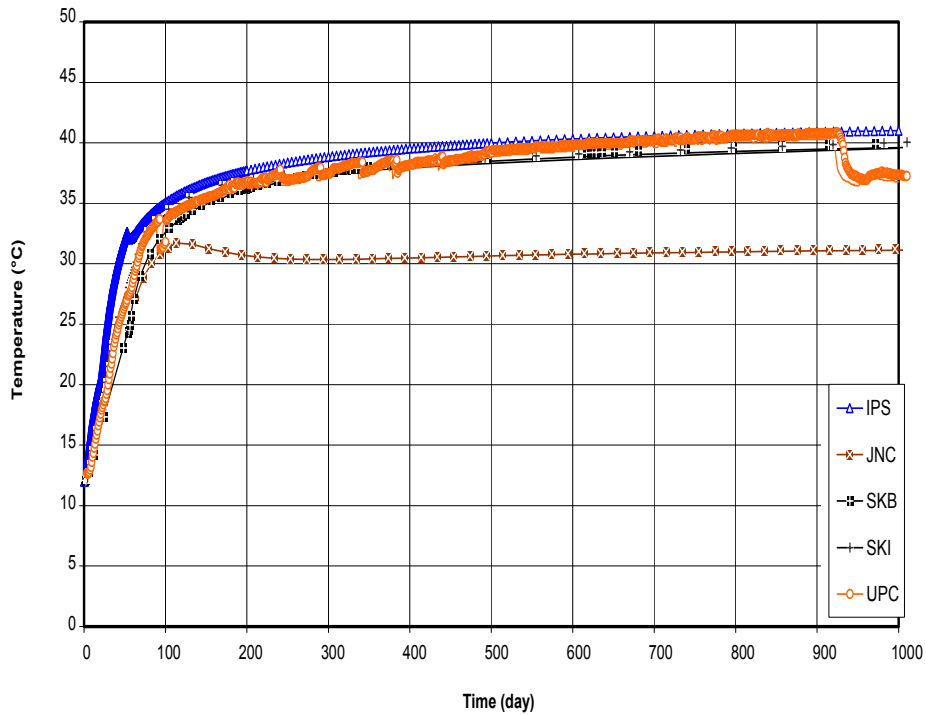


Figure 8.6b: Measured and predicted evolutions of temperature in borehole SF21 at point 1 ( $r = 1.20$  m).

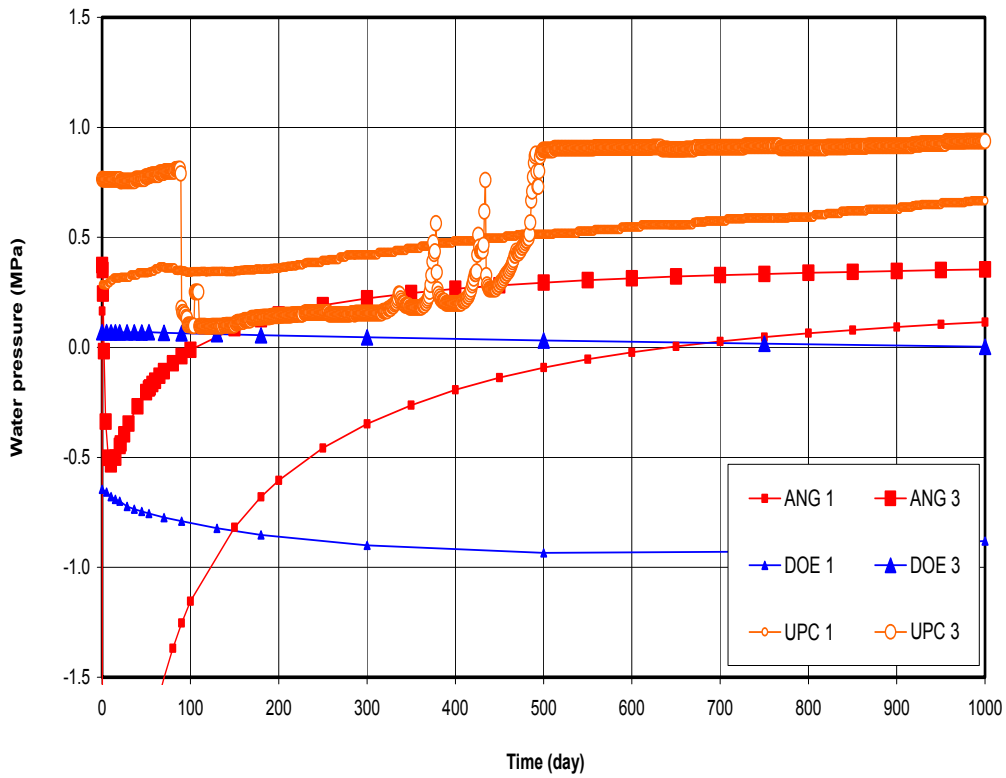


Figure 8.7a: Measured and predicted evolutions of water pressure in borehole SF21 at point 1 ( $r = 3.03$  m) and at point 3 (13.06) m.

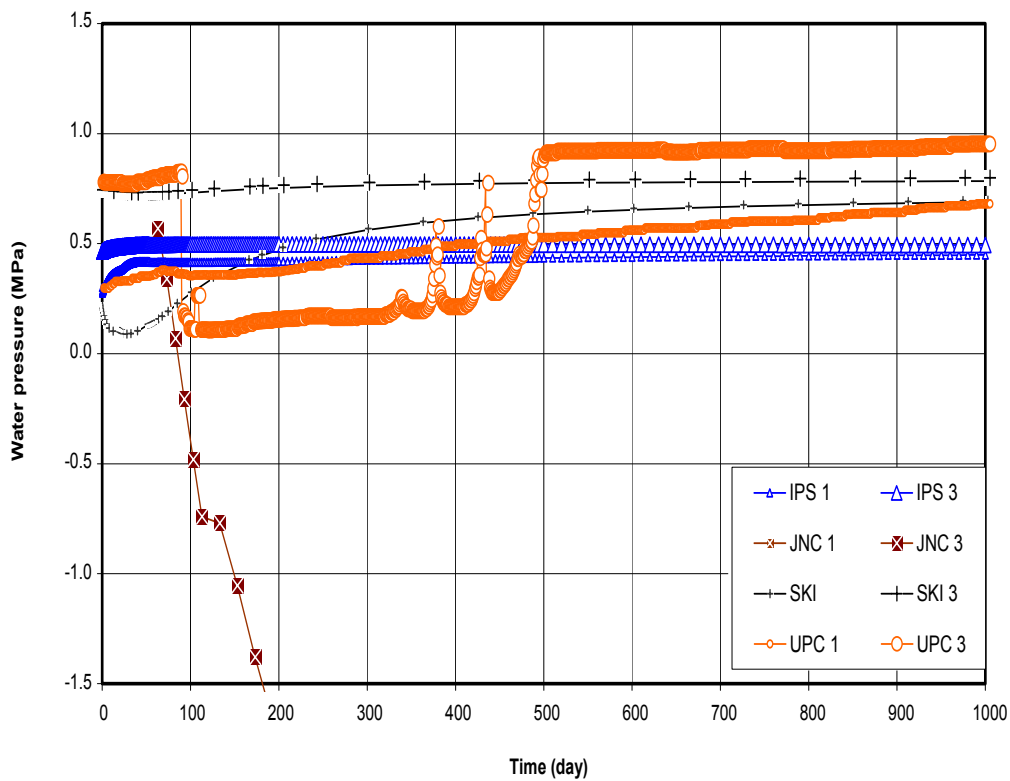


Figure 8.7b: Measured and predicted evolutions of water pressure in borehole SF21 at point 1 ( $r = 3.03$  m) and at point 3 (13.06) m.

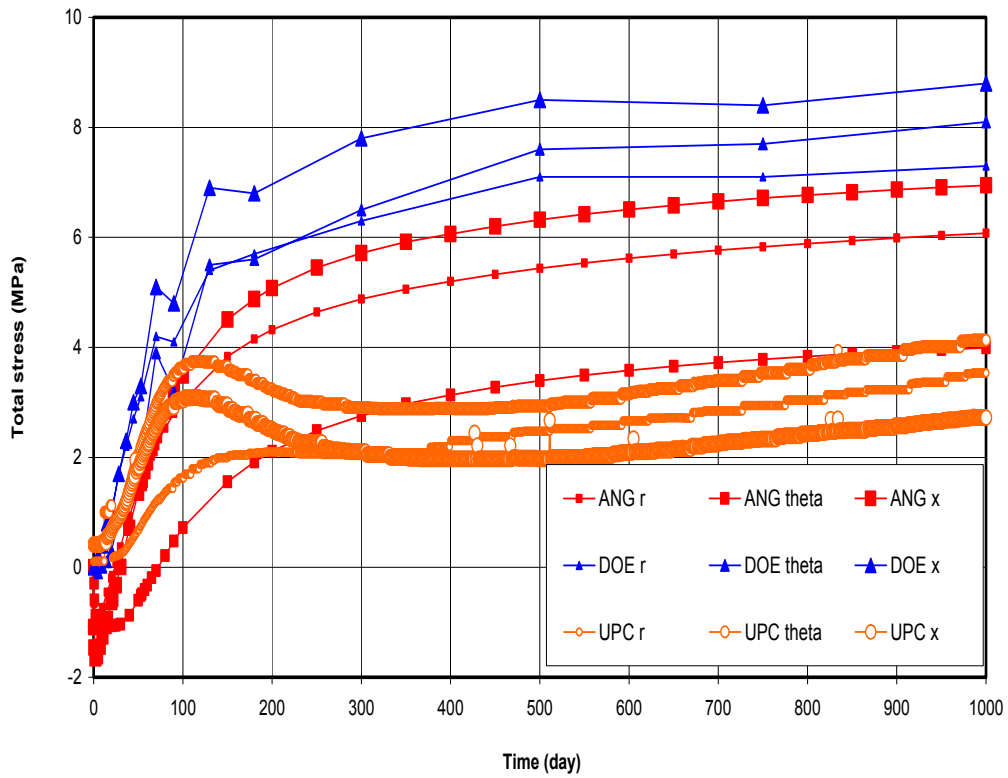


Figure 8.8a: Measured and predicted evolutions of total stress components in borehole SG2 at points 1, 2 and 3 ( $r \approx 3.0$  m).

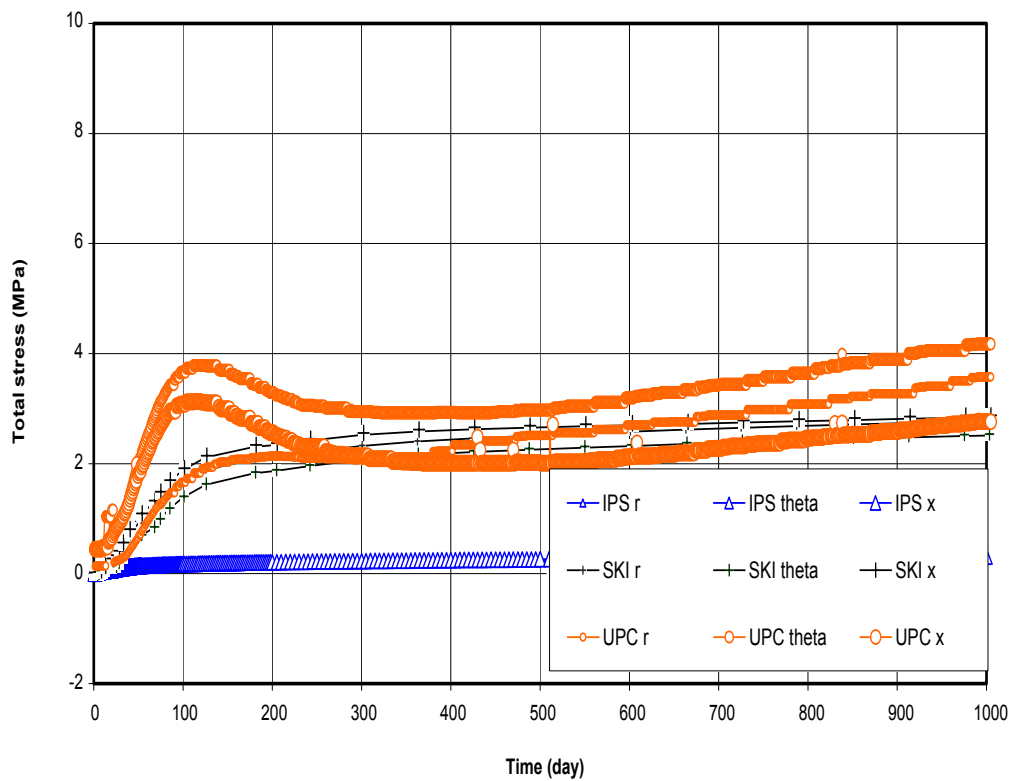


Figure 8.8b: Measured and predicted evolutions of total stress components in borehole SG2 at points 1, 2 and 3 ( $r \approx 3.0$  m).

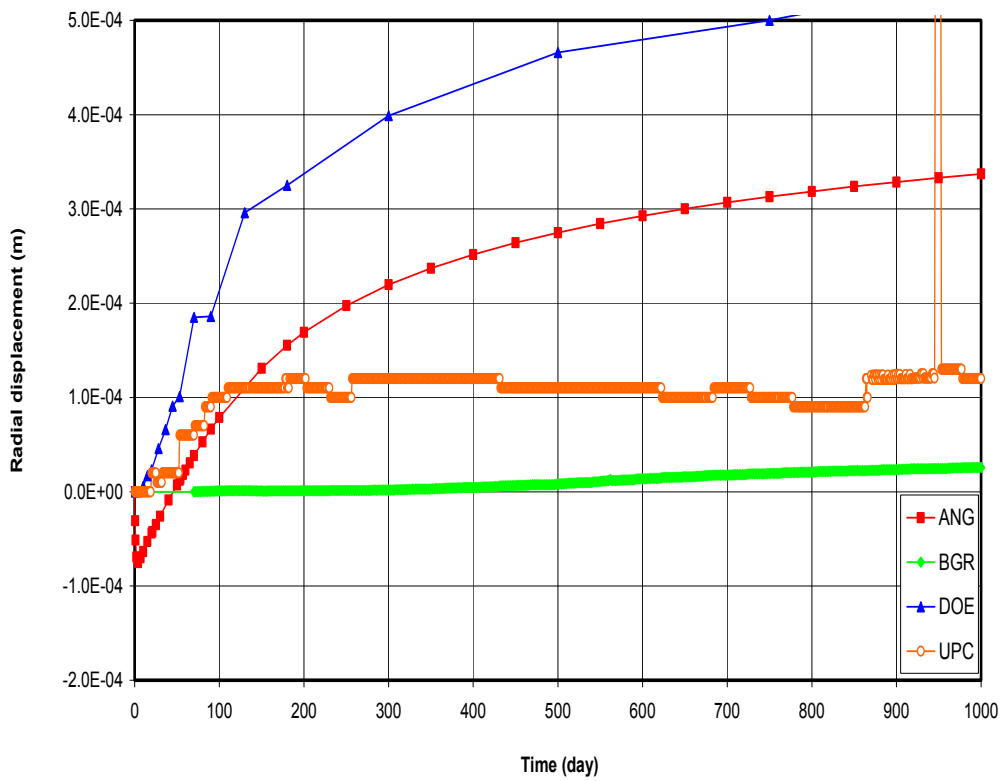


Figure 8.9a: Measured and predicted evolutions of radial displacements in borehole S11 at point 3 ( $r = 8.03$  m).

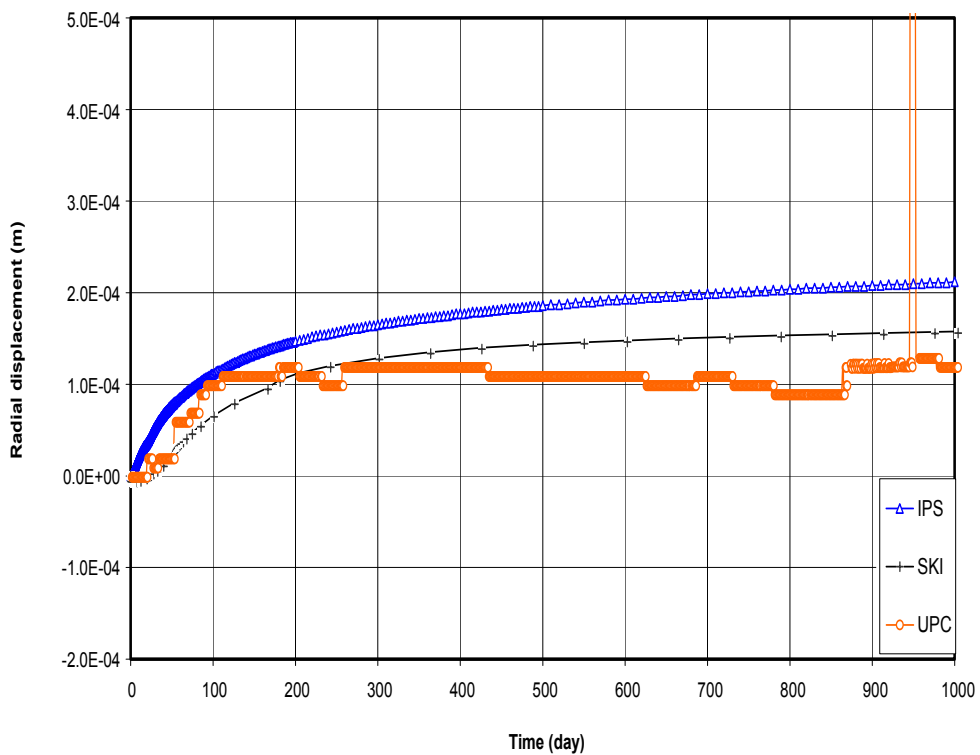


Figure 8.9b: Measured and predicted evolutions of radial displacements in borehole S11 at point 3 ( $r = 8.03$  m).

develop higher pore water pressures that points deeper in the rock, because the former will experience a larger temperature increase. On the other hand, if the natural gradient-induced flow dominates, points located at increasing radial distances will tend to show higher pore water pressures. Bentonite suction will tend to enhance this second effect and may even induce negative pore pressures in the granite under certain circumstances. In fact, the interaction between granite and buffer in the proximity of the interface is not a straightforward phenomenon. Important qualitative differences in behaviour may be explained by relatively minor changes of the bentonite and the granite. A sensitivity analysis of the behaviour of this interface is given in Gens et al. (1998b).

It has been suggested that the limited transient reaction of the pore water pressure in the Grimsel host rock is a natural consequence of the high permeability of the rock and, to a lesser extent, of the averaging effect of the measuring interval (a few meters of borehole). The records of packer water pressures have provided interesting complementary evidence of the transient pore water pressure development. Also, the evolution of total stresses, 3 m away from the tunnel wall, shows a transient initial peak which has also been attributed to excess pore water pressure behaviour.

The measured pressure response at  $r = 13.06$  m in boring SF21 is unfortunately not conclusive because of the abnormal fall of pressure recorded during a relatively long period ( $t = 80$  to 480 days). Some transient increases recorded during this period and the readings during the second half of the considered period tend to show that the actual water pressure in the rock at the sensor position increases steadily from an initial value of 0.75 MPa to final values of 0.9 MPa. This is a pressure higher than the recorded value at  $r = 3.03$  m (0.3 to 0.7 MPa). No transient changes of pressure were recorded in this transducer, which is close to the bentonite-rock interface. This data is interpreted as an indication that the distribution of pore water pressure in the rock is mainly controlled by a pure radial flow induced by hydraulic gradients. No indication of negative (or, indeed, a transient decrease in pore pressure) was detected in the granite. The interpretation is that the suction of the bentonite had in this case a negligible effect. This is also a consequence of the relatively high value of the granite matrix permeability and the small flow rates required to progressively hydrate the bentonite.

Some of the model's results favour this interpretation (SKI, JNC and SKB- although it calculated some initial negative values of water pressure at the transducer close to the bentonite interface). In an extreme position is the case of ANG, who predicted very dominant suction-induced effects. In general, none of the modelling teams predicted temperature-related water pressure effects, a fact which is explained by the rock permeability, already calibrated during the first part of the benchmark exercise. Long-term water pressures increase slowly with time in the tunnel immediate vicinity (a few meters). Measured water pressures after 1000 days of test operation are, however, relatively small (1MPa).

Measured stresses correspond to changes experienced after cell installation, once the Febex tunnel was excavated. Therefore, they measured total stress increments induced by temperature changes and, to a lesser extent, by the swelling of the bentonite. The most distinctive feature of the stress records is the peak values recorded in all three values of stress ( $\sigma_r$ ,  $\sigma_\theta$ ,  $\sigma_x$ ) measured in borehole SG2 at an early stage (100 days). The fact that the stresses decreased later in the period  $t = 100$  days to  $t = 400$  days, to increase slowly at increasing times, suggests that the stress cells measured a transient change in pore water pressure induced by the increase in temperature. The subsequent reduction of total stress reflects the dissipation of excess pore water pressure. This behaviour also indicates that the system used to measure pore water pressures (isolated stretches of boreholes by means of packers) is not suitable to record point values. The

measured pressure in a borehole interval is the average of “point” pressures. In addition, any highly conductive feature crossing a measuring borehole interval would reduce fast any temperature-induced increase in pressure. On the other hand, the stress cells tend to provide point measurements and they are well suited to detect local changes.

None of the models predicted the recorded peak of total stress. This is, of course consistent with the calculated pore water pressures, discussed previously. Some of the teams (CNS, ANG, DOE) overestimated the measured stresses. Others (SKI, SKB, BGR) reported values closer to actual data (2 – 4 MPa at early times and 3-4 MPa at the end of the measuring period). The analysis presented of the mean and deviatoric components of the stress state indicates that the stress increment has a dominant isoropic component. The analysis is only approximate since stresses were not recorded exactly at the same point.

Measured displacements are a consequence of the temperature increase. In view of the high granite stiffness the recorded displacements between an anchored point within the boring SI-1 at a radial distance of 8.03 m and the tunnel wall is very small (0.1 mm) and close to the precision of the measuring system. Most of the teams overestimate this value but SKI reported a very good prediction.

## 8.6 Final remarks

The FEBEX test is one of the few large-scale tests available to gain an integrated perspective of the behaviour of current concepts for nuclear waste disposal in crystalline rock. The comprehensive instrumentation installed in the rock and in the compacted bentonite buffer has yielded vast amounts of data over the past six years. Part of this data, the data corresponding to the first three years of heating, has been used to conduct a Benchmark exercise to evaluate the capabilities of a number of finite element codes developed to handle coupled problems in geological and porous media. This Report provides an account of the main results achieved during the performance of the exercise. Some selection of the large amount of results has been unavoidable.

For the purposes of the organization of the exercise into specific tasks the Benchmark was divided into three main parts: A: Rock behaviour during the excavation of the FEBEX tunnel, B: Buffer behaviour and C: Rock behaviour during the heating and (partial) hydration of the buffer. This distribution has been maintained in the organization of the Report.

Specific conclusions for each of the mentioned parts have been given before. Only a few concluding remarks will be added here:

- The best predictions of the water inflow into the excavated tunnel are found when the hydro geological model is properly calibrated on the basis of other known flow measurements in the same area. The particular idealization of the rock mass (equivalent porous media, discrete fractures) plays a secondary role
- The development and dissipation of excess pore water pressures in the vicinity of the advancing tunnel (at the time of the FEBEX tunnel excavation) was a clear example of hydro-mechanical interaction. It was concluded that the development of pore pressures was controlled by the initial stress field state, by the rate of excavation and by the permeability and drainage properties of the granite. However, the available information on the intensity and direction of principal stresses in the area was found inconsistent with the actual measurements. The problem posed by this discrepancy was essentially unsettled since a precise

determination of the initial stress state in the vicinity of the FEBEX tunnel was not available.

- Predicting the behaviour of the buffer under the combined heating and wetting actions requires a fully coupled THM formulation, which incorporates all the necessary physical processes controlling the bentonite behaviour. Only a partial set of codes could offer the required features. Particularly relevant to predict the early stages of heating was the inclusion of phase changes of water and the vapour transport. Codes incorporating these features were capable of making good predictions. It should be added that the FEBEX in situ test benefits from a comprehensive experimental information on compacted bentonite properties derived from a large variety of laboratory tests on samples and on small-scale hydration and heating cells.
- It has been shown that the hydration of the bentonite buffer was essentially independent of the heterogeneous nature of the rock hydraulic conductivity features. This is explained by the fact that the rock matrix permeability is higher than the saturated bentonite permeability. Some 3D analyses performed, where the heterogeneous permeability features of the rock have been included, tend to support also this conclusion.
- The heating of the rock resulted in a significant increase in rock stresses in the vicinity of the FEBEX tunnel. Water pressures remained however essentially unchanged. The relatively high rock permeability explains the absence of significant pore water pressure transients. Only one of the participating modelling teams was capable of achieving a consistent prediction of all the measured variables in the rock: temperature, water pressures, rock stresses and radial displacements

## 9. Concluding remarks

The FEBEX test is one of the few large-scale tests available to gain an integrated perspective of the behaviour of current concepts for nuclear waste disposal in crystalline rock. The comprehensive instrumentation installed in the rock and in the compacted bentonite buffer has yielded vast amounts of data over the past six years. Part of this data, the data corresponding to the first three years of heating, has been used to conduct a Benchmark exercise to evaluate the capabilities of a number of finite element codes developed to handle coupled problems in geological and porous media. This paper provides an account of the main results achieved during the performance of the exercise. Some selection of the large amount of results has been unavoidable. A description of the hypotheses and specific features of the different codes participating is also outside the scope of this paper. However, a few companion papers provide a detailed insight into some of the models and computer tools participating in the Benchmark.

For the purposes of the organization of the exercise into specific tasks the Benchmark was divided into three main parts: A: Rock behaviour during the excavation of the FEBEX tunnel; B: Buffer behaviour and C: Rock behaviour during the heating and (partial) hydration of the buffer. This distribution has been maintained in the paper.

A discussion for each of the mentioned parts has been given before. Only a few concluding points will be added here:

The best predictions of the water inflow into the excavated tunnel are found when the hydro geological model is properly calibrated on the basis of other known flow measurements in the same area. The particular idealization of the rock mass (equivalent porous media, discrete fractures) plays a secondary role.

The development and dissipation of excess pore water pressures in the vicinity of the advancing tunnel (at the time of the FEBEX tunnel excavation) was a clear example of hydro-mechanical interaction. It was concluded that the development of pore pressures was controlled by the initial stress field state, by the rate of excavation and by the permeability and drainage properties of the granite. However, the available information on the intensity and direction of principal stresses in the area was found inconsistent with the actual measurements. The problem posed by this discrepancy was essentially unsettled since a precise determination of the initial stress state in the vicinity of the FEBEX tunnel was not available.

Predicting the behaviour of the buffer under the combined heating and wetting actions requires a fully coupled THM formulation, which incorporates all the necessary physical processes controlling the bentonite behaviour. Only a partial set of codes could offer the required features. Particularly relevant to predict the early stages of heating was the inclusion of phase changes of water and of vapour transport. Codes incorporating these features were capable of making good predictions. It should be added that the FEBEX in situ test benefits from a comprehensive experimental information on compacted bentonite properties derived from a large variety of laboratory tests on samples and on small-scale hydration and heating cells.

It has been shown that the hydration of the bentonite buffer was essentially independent of the heterogeneous nature of the rock hydraulic conductivity features. This is explained by the fact that the rock matrix permeability is higher than the saturated bentonite permeability. Some 3D analyses performed, where the heterogeneous permeability features of the rock have been included, tend to support also this conclusion.

The heating of the rock resulted in a significant increase in rock stresses in the vicinity of the FEBEX tunnel. Water pressures remained however essentially

unchanged. The relatively high rock permeability explains the absence of significant pore water pressure transients. Only one of the participating modelling teams was capable of achieving a consistent prediction of all the measured variables in the rock: temperature, water pressures, rock stresses and radial displacements.

# References

- Amiguet J.-L. *Grimsel Test Site. Felskennwerte von intaktem Granit.*  
Zusammenstellung felsmechanischer Laborresultate diverser granitischer Gesteine.  
NAGRA, NIB 85-08, Sep. 1985.
- Bräuer V., Kilger B., and Pahl A. *Grimsel Test Site. Engineering geological investigations for the interpretation of rock stress measurements and fracture flow tests.* NAGRA, NTB 88-37E, Apr. 1989.
- Falk L., Magnusson K.-Å., Olsson O., Ammann M., Keusen H.R. and Sattel. *Grimsel Test Site. Analysis of radar measurements performed at the Grimsel Rock Laboratory in October 1985.* NAGRA, NTB 87-13, Feb. 1988.
- Fierz T. *FEBEX Instrumentation of BOUS 85.001 and 85.002, FBX 95.001 and 95.002 radial boreholes.* Solexperts AG, 1008, Jul. 1996.
- Finsterle S. and Pruess K. *Solving the estimation-identification problem in two-phase flow modelling.* Water Resour. Res., 31(4), 913-924, 1995.
- Gens, A. *The role of Geotechnical Engineering for nuclear energy utilisation.* In Vaniček et al. (eds.) Proc. XIII ECSMGE (25-28.08.2003, Prague), Special Lecture 2, Vol. 3, 25-67, Prague. 2003.
- Gens, A., García-Molina, A., Olivella, A., Alonso E. E. and Huertas, F. *Analysis of a full scale in situ test simulating repository conditions.* Int. J. Numer. Anal. Meth. Geomech., **22**, 515-548. 1998a.
- Gens, A., Guimaraes, L. N., García-Molina, A. J. and Alonso, E. E. *Interaction between clay barrier and host medium in radioactive waste isolation.* In: *Environmental Geotechnics.* Balkema. 1: 581-588. 1998b.
- Guimerà J., Ortuño F., Vázquez E., Ruiz B., Martínez L., Carrera J. and Meier P. *Pulse tests at "in drift" boreholes. Performance and evaluation.* UPC, 70-UPC-L-0-1001, Sep. 1996.
- Guimerà J., Carrera J., Martínez L., Vázquez E., Ortuño F., Fierz T., Bülher C., Vives L., Meier P., Medina A., Saaltink M., Ruiz B. and Pardillo J. *FEBEX hydrological characterization and modelling.* UPC, 70-UPC-M-0-1001, Jan. 1998.
- Häring M.O. *GTS/FEBEX: Supervision and interpretation of geophysical investigations Boreholes FBX95.001 and FBX95.002.* NAGRA, NIB 96-14.
- Keusen H.R., Ganguin J., Schuler P. and Buletti M. *Grimsel Test Site. Geology.* NAGRA, NTB 87-14E, Feb. 1989.
- Meier P., Fernández P., Carrera J. and Guimerà J. *FEBEX - PHASE 1. Results of hydraulic testing in boreholes FBX 95.001, FBX 95.002, BOUS 85.001 and BOUS 85.002.* UPC, Dec. 1995.
- Pahl A., Heusermann St., Bräuer V. and Glöggler W. *Grimsel Test Site. Rock stress investigations.* NAGRA, NTB 88-39E, Apr. 1989.
- Pardillo J. and Campos R. *FEBEX - Grimsel Test Site (Switzerland) Considerations respect to the fracture distribution.* CIEMAT, 70-IMA-L-2-05, Mar. 1996.
- Pardillo J., Campos R. and Gimerà J. *Caracterización geológica de la zona de ensayo FEBEX (Grimsel - Suiza).* CIEMAT, 70-IMA-M-2-01, May 1997.
- Pintado X. *Ensayos THM para el Proyecto FEBEX realizados por la UPC-DIT.* UPC, 70-UPC-M-0-03, October 2000.
- Pintado X. and Lloret A. *THM laboratory tests in FEBEX Phase 3.* UPC, 70-UPC-L-3-01, Dec. 1997.
- Rutqvist, J., Rejeb, A., Tijani M. and Tsang, C.-F.. *Analyses of coupled hydrological-mechanical effects during drilling of the FEBEX tunnel at Grimsel.* In O. Stephansson, J.A. Hudson and L. Jing (Editors) Proc. of GeoProc 2003 (Stockholm,

- 13-15.10.2003), pp. 114-119. Stockholm, Sweden. 2003.
- Schneebeli M., Flühler H., Gimmi T., Wydler H. and Läser H.-P. *Measurements of water potential and water content in unsaturated crystalline rock*. *Water Resour. Res.*, 31(8), 1837-1843, 1995.
- Villar M.V. *Ensayos THM para el Proyecto FEBEX*. CIEMAT, 70-IMA-L-0-66, March 1999.
- Voborny O., Adank P., Hürlimann W., Vomvoris S. and Mishra S. *Grimsel Test Site. Modelling of groundwater flow in the rock body surrounding the underground laboratory*. NAGRA, NTB 91-03, Oct. 1991.

[www.ski.se](http://www.ski.se)

**STATENS KÄRNKRAFTINSPEKTION**  
Swedish Nuclear Power Inspectorate

**POST/POSTAL ADDRESS** SE-106 58 Stockholm

**BESÖK/OFFICE** Klarabergsviadukten 90

**TELEFON/TELEPHONE** +46 (0)8 698 84 00

**TELEFAX** +46 (0)8 661 90 86

**E-POST/E-MAIL** [ski@ski.se](mailto:ski@ski.se)

**WEBBPLATS/WEB SITE** [www.ski.se](http://www.ski.se)